Elastic Waves for Damage Detection in Structures

Wieslaw Ostachowicz[*] and Pawel Kudela

[*] Faculty of Navigation,
Gdynia Maritime University, Gdynia, Poland
[‡] Department of Mechanics of Intelligent Structures,
Polish Academy of Sciences, Gdansk, Poland

Abstract The main issues regarding damage detection in elements of structures are discussed in the particular case that the detection is conducted by the use of methods based on the phenomenon of elastic wave propagation. The emphasis is placed on modelling the phenomenon of elastic wave propagation in composite elements of structures, along with issues of wave interactions with damage and problems of damage location.

1 Introduction to SHM Methods Based on the Phenomenon of Elastic Wave Propagation

The scope of *Structural Health Monitoring* (SHM) includes constant monitoring of the structure's material condition (in real-time), for the elements of the structure as well as for the whole structure during its useful lifetime. The condition of the structures material is required to remain within the limits specified by the standards of the design process. Those standards, regarding the material, ought to take into consideration changes caused by standard exploitation wear during the operation process, changes caused by environmental conditions, in which the structure is being used, and coincidental situations influencing the condition of the material. Owing to the fact that the monitoring process is being conducted continuously during operation, there will be a record of the complete history of utilisation. Such information may be used for future condition prognosis as well as prediction of faults and the structure's safe utilisation time.

According to a number of publications, SHM is being defined as a new approach to non-destructive inspection of a structure (also called Non-Destructive Testing/Evaluation - NDT/E). The innovation of this approach is based on the continuous monitoring of the material's condition during

the exploitation process of the device. It requires certain structural and utilisation solutions distinctive for this new discipline.

SHM is combined of such disciplines as sensorics, IT, electronics (especially microprocessor technology), mechanics and materials engineering. The effect of synergy is achieved by combining former disciplines, and it enables raised safety levels of the structure's utilisation along with lowering of the maintenance expenses.

Systems executing SHM processes ought to be structure integrated; this allows insertion of changes into the structure in such a way that the probability of a failure is minor. It also enables minimisation of the failure risk through management of the structure's utilisation and treating it as part of a bigger system. The first layer of a SHM system is the monitoring layer specified by the type of physical phenomenon that is being monitored by the sensors. It is dependent on the damage type to be detected and the type of physical phenomenon that is being used by the sensors in order to generate the signals (mostly electrical) containing features and processable information regarding damage. Several (perhaps up to a few dozen) connected sensors can work together in a system measuring environmental factors influencing the condition and process of the exploitation of the structure. Data gathered from all the sensors along with historical data from previous structures allow diagnostic synthesis of information (*signal fusion*) regarding the condition of the structure. Once the above-mentioned information is linked with all the data from the general system of knowledge about the phenomenon of damage and structural wear, it is possible to gain prognosis of condition and data defining the scope of any necessary repair. It is now common for such purposes that simulation systems are used; such systems enable extremely quick generation of results, similar to those obtained from the chain of sensors based on familiar damage models (virtual exploitation of the structure).

The motivation for applying such systems is:

- ability to avoid failures with catastrophic consequences;
- ability to optimise the utilisation process (minimisation of emergency stoppage time);
- gaining essential information for designers regarding structural modification;
- ability to minimise maintenance costs and to raise the efficiency of a device thanks to the use of a methodology of repair according to condition, as well as avoiding disassembly, and replacement of non-damaged and non-used elements;
- ability to avoid operator mistakes regarding evaluation of the condition of the structure.

The systems mentioned are being used for air force and aviation, military equipment, construction industry infrastructure, and machines crucial for industry (e.g. power industry, chemistry, etc.). An extremely important factor influencing the common use of SHM systems is the economical factor. The justification may be found in several papers and it lies in comparing maintenance costs with the efficiency of the structure. For the structure without SHM systems installed, costs rise along with the utilisation time and at the same time efficiency drops. Installation of SHM systems potentially enables one to fix maintenance costs with equally fixed efficiency of the structure. However, one condition of applying SHM systems must be met; this condition limits the general ability of putting them into practice i.e. the cost of the system itself ought to be lower than the positive economical effect connected with its application.

The necessity of reducing the cost of SHM systems is nowadays connected with the application of intelligent materials and structures; they enable integration of the structure and the built-in sensors into one system. In order to be effective, such actions must be taken during the stage of designing of the structure.

From the beginning of the 80's, a tendency towards intelligent structure applications are were observed, especially in aviation and construction industry. Their characteristic feature is adaptation of those structures to the exploitation conditions. In intelligent structures, this adaptation takes place autonomically. Within the range of intelligent structures, distinctions can be made as follows: structures sensitive to utilisation conditions, structures controlled within the range of their properties, and auto-adaptative structures that adjust their properties to their utilisation needs. In practice, homogeneous materials commonly used in structures are being replaced by composite materials or other multi-materials (materials composed of layers of various physical properties). Within the range of materials and intelligent structures one can distinguish structures of adjustable geometry (shape), structures with adjustable vibration behaviour and structures with adjustable condition. In particular, the last type of structure is constantly in use with SHM techniques. Most often, intelligence is expressed through structure-integrated sensors made from intelligent materials (*embedded sensors*) or executive modules (*embedded actuators*), for which the task is to identify defects and alleviate the effects of failure. Operation of such modules depends on generating deformations of the structure in such a way as to decrease stresses in these areas of concentration. Nowadays, the search for phenomena, and methods of their measurement, which enable continuous monitoring of structural condition through monitoring of the condition of its material, continues.

Research on the development of SHM systems is very often inspired by discoveries in the fields of biology and living organisms (*biomimetics*). Very similar research is being conducted in the fields of medicine and SHM method development. SHM systems find application not only in the life-time of the structure but also in the time of its production, transport and installation. They also enable proper management of the structure's wear, through suitable choice of missions that must be executed, and service actions required for safe meeting of given criteria. Methods that could be used as the most economically effective and durable, in every stage of the product usage, are still being searched for.

To put it briefly, the foregoing survey regarding SHM allow one to say that it is a new interdisciplinary area, gathering such sciences as mechanics, materials engineering, electronics, computer science, physics, optics and many others. This area has applications in the utilisation of structures in aviation, construction industry, motor industry and power industry including those connected with nuclear power. The spectrum of applications is constantly expanding. Among the many methods used in SHM systems, one can distinguish between active or passive methods. In the passive methods, one can observe signals generated by the structure's inbuilt sensors and on this basis, the condition can be evaluated. Active methods depend on forcing disturbances by the use of properly inbuilt executive cores that cause structural responses, measured by sensors. On the basis of response signals registered by the sensors, the condition is evaluated. Some of the widespread SHM methods are those based on structural vibration measurement. Among them: symptomatic methods, in which the symptoms of damage are certain estimators from the signals of structural response, or model-based methods, where the symptoms of damage are parameter changes or changes to the structure of a model.

Many methods used in practice to build SHM systems are being adopted from widely-known and applied disciplines e.g. NDT. Classical NDT methods can be executed continuously, such as: measurement of acoustic emission, Lamb waves, temperature, or mechanical impedance or direct monitoring of the displacement field with the use of visual methods; all these are examples of applying NDT techniques in SHM systems. In those kinds of solution, two sets of methods may be distinguished: methods where the sensors are integrated with the structure and non-contacting methods. The latter have wider application owing to miniaturisation and the costs of SHM system installation.

One of such methods, that can be applied passively as well as actively, and where the measurements are executed in a non-contacting way, is the method based on examination of thermo-flexibility phenomena accompany-

ing damage, especially its formation and propagation. Currently, interest in this method is increasing due to the opportunity of non-contact measurements of thermal phenomena within structures and intensive development in temperature measurement. Another method is the method of surface Lamb wave excitation within the structure. This method uses a grid of sensors/actuators. Registration and processing of transmitted waves as well as reflected waves is conducted. Evaluation of the condition of the structure takes place on the basis of wave profile deformations due to damage in the interrogated area of the structure.

A different method is one based on parameters of modal models of the monitored structure. One very effective method is the modal filter method and the statistical evaluation of detected changes in the model. More and more common, is the application of scanning pictures for evaluation of structural deformation. In this way, one may monitor static as well as dynamic changes. Depending on measurement requirements, methods using laser beam are applied (strain methods, holographic methods, and interferometry methods characterised by nanometer sensitivity of measurements of displacement fields) or non-coherent light methods (fotogrametric methods, the picture correlation method, moiré pattern techniques and pattern projection techniques). The most commonly-used technique of picture processing is correlation of images of non-deformed and deformed structures. Contemporary techniques of image measurement and recording enable monitoring of even minor changes in the condition of the structure owing to applications of the so-called phase methods of analysis of pattern images or subpixel techniques in fotogrametric methods or methods of picture correlation. Contemporary quick cameras enable recording of dynamic changes of deformation with frequencies up to 32000 Hz. Pulse laser sources of light enable transmission of highly sensitive interferencial methods from the lab, directly to the studied structure. In new structures, where utilisation safety is of the greatest importance, sensors in the form of intelligent materials, piezoelectrics and optical fibres (*fibre Bragg gratings*), are currently embedded; they become an inseparable part of the structure and continuously gather information about the structure's fatigue limit and condition of the material. This enables prediction of properties, estimation of time of safe utilisation and evaluation of planned repair ranges. As presented in the review of current knowledge, investigations conducted using SHM techniques are more and more precise and enable evaluation of condition within the range of local changes, especially, in the degradation of structural material. This enables more and more accurate predictions of the condition of the structure during its lifetime.

2 Modeling of Structural Stiffness Loss Due to Damage

Fatigue cracking and delamination are particularly dangerous and, at the same time, the most common kinds of damage in elements of machines and structures. It is of great importance for safe operation to ensure that elements of machines and structures are free of any fatigue cracks and delaminations and in the case of their presence, to determine their extent. Since existing non-destructive methods for detection of fatigue cracks and delaminations fail in many practical cases, vibration methods in diagnosis of such damage have been continuing for nearly twenty years. These methods are based on diagnostic relations between the size and location of failures and changes in some dynamic characteristics of constructional elements. In order to establish such relations and to identify changes of the dynamic characteristics, efficient models that facilitate the assessment of the influence of fatigue cracks and delaminations must be established. A review of the existing models used for analysis of the influence of fatigue cracks and delaminations on changes in dynamic characteristics of constructional elements is presented in this section.

2.1 Discrete models

In general, discrete models of fatigue damage are not restricted geometrically. Such restrictions are one of the biggest disadvantages of the continuous or discrete–continuous models. In order to create a discrete model of a constructional element with a fatigue crack, the Finite Element Method (FEM) is most usually applied. Although other methods like the boundary element method, graph method, transition matrix method and the analogue method are also used, these methods are not as popular and commonly used as the finite element method.

The simplest method applied to model constructional elements with fatigue damage is based on the use of classical finite elements. In this case a fatigue crack in the finite element is modelled by reduction of elastic coefficients of the element (Cawley and Adams, 1979), by reduction of its Young's modulus (Yuen, 1985), and by reduction of the cross–sectional area of the element at the crack position (Bachschmid et al., 1984). The main disadvantage of these approaches is the fact that the reduced parameters describing a fatigue crack are chosen arbitrarily. Generally, their values are not directly related to the actual size of a crack and due to that fact, a precise study of the influence of the crack depth on changes in dynamic characteristics cannot be made. The singular character of the stress and strain fields around the crack tip is also neglected in these methods.

In the last decade, new FEM-based models have been formulated. Some authors have assumed that the failure appears inside a special finite element (Ostachowicz and Krawczuk, 2001). A model of a truss finite element with an open one–sided transverse crack has been developed by Krawczuk (1992). Models of beam finite elements with fatigue cracks of different types can be found in the work of Haisty and Springer (1988), Gounaris and Dimarogonas (1988), Chen and Chen (1988). Krawczuk and Ostachowicz (1993b) investigated a mathematical, FEM-based model of a beam with a crack, loaded at the end with a constant tensile axial force; the authors assumed that the crack does not propagate and remains open during the beam's vibrations. Assumption of a complete opening of the crack in this case was correct because the beam was subjected to the action of a constant axial force.

Ostachowicz and Krawczuk (1992) also developed a model of a rotor shaft of constant cross–section with a crack. The shaft was modelled by finite elements; the crack was considered to be open. The stiffness matrix for the element with the crack was formulated. The model took into consideration the torsional–bending interaction in the rotor vibration.

The curved-beam finite element with a transverse, one-edged, nonpropagating, open crack has been investigated by Krawczuk and Ostachowicz (1997). The authors presented an analysis of the effect of the crack position and location on the changes of the in–plane natural frequencies and mode shapes of the clamped–clamped arch. The authors assumed that the crack only changes the stiffness of the element, with the mass of the element remaining unchanged. The investigated model of the cracked element was restricted to curved beams with rectangular cross–section.

A cracked-beam finite element that is based on elasto–plastic fracture mechanics has been formulated by Krawczuk et al. (2000, 2001). Crack tip plasticity at the cracked cross-section was included in the model of the local flexibility. The inertia and stiffness matrices took into account the effect of flexural bending deformation due to the crack presence; they were formulated in closed form.

Apart from one–dimensional models, special models of two or three–dimensional constructional elements with fatigue cracks have been also investigated. The cracks occurring in a plate can be modelled by the finite element method in various ways. Plate finite elements with fatigue cracks have been used by Qian et al. (1991), Krawczuk (1993), and Krawczuk and Ostachowicz (1994), while a solid finite element with a fatigue crack has been developed by Krawczuk and Ostachowicz (1993a), and a shell element by Krawczuk (1994).

Krawczuk (1993) presented a method of creating the stiffness matrix of

a finite plate element with a non-propagating, internal open crack. The method is similar to the one described by Qian et al. (1991) but contrary to their approach, the stiffness matrix of the cracked element was given in closed-form. The additional flexibility matrix was calculated by taking into account the additional elastic stress energy due to the occurrence of the crack in the plate. The method is restricted to cracks whose length is smaller than the dimensions of the element; It is assumed that the crack changes only the stiffness of the element and the mass of the element remains unchanged.

A method of creating the stiffness matrix of a hexahedral eight–node finite element, with a single, nonpropagating, transverse, single-edge crack at half of its length, has been investigated by Krawczuk and Ostachowicz (1993a). The crack was modeled by adding an additional flexibility matrix to the non-cracked element. The terms of the additional matrix have been calculated by the use of an approximate model of the stress intensity factor.

Many researchers have studied damage models in composite structures extensively. Krawczuk et al. (1997) proposed the formulation of a finite composite beam element with an open crack. The damaged part of the beam was modelled by a special finite element with a crack, while the undamaged part was substituted by three-node beam element. The crack is placed in the middle of the element and remains open. The element has three nodes; each of them has two degrees of freedom: transverse displacements and rotations. In the paper (Krawczuk et al., 1997), only the case of flat bending was considered.

Krawczuk et al. (1997) have investigated a model of a layered, delaminated composite beam. The beam was modelled by beam finite elements with three nodes and three degrees of freedom per node. In the delaminated region, additional boundary conditions were applied. It was assumed that the delamination was open (i.e. the contact forces between lower and upper parts are neglected). The delaminated region was modelled by three finite elements connected at the delamination crack tip where additional boundary conditions were applied. Each element had three nodes with three degrees of freedom: axial displacements, transverse displacements, and the independent rotations. In addition to general conditions of beam theory, it was assumed that the extensional and bending stiffness were uncoupled.

A model of a finite delaminated plate element has been developed by Żak et al. (2000); Zak et al. (2001). The delamination was modelled by three plate finite elements and to connect them, additional boundary conditions were applied at the delamination front. Each finite element had eight nodes with five degrees of freedom per node. Later papers (Krawczuk and Ostachowicz, 2002; Ostachowicz et al., 2002, 2003; Zak et al., 2003) present

results for the identification of the location of failures in both isotropic and composite structures by means of a genetic algorithm search technique based on changes in natural frequencies. The location and size of failures are determined by minimisation of an error function which expresses the difference between calculated and measured natural frequencies.

Laboratory experiments have been conducted to ensure the reality of analytical and numerical models; the results obtained are promising, particularly because they have confirmed investigated models. Results of experimental tests have been presented in (Krawczuk et al., 2000, 1997; Żak et al., 2000; Ostachowicz et al., 2003; Zak et al., 2003).

3   Lamb Waves

Elastic waves that propagate in solid media bounded by two free and parallel surfaces are known in the literature as Lamb waves or guided waves. Lamb waves are named after Horace Lamb in honour of his fundamental contributions in this area of research. Lamb developed a mathematical theory that describes this kind of elastic waves, but interestingly he never managed to generate this type of wave in a real structure. Lamb waves propagate both as symmetric (S0, S1, S2, . . .) and antisymmetric (A0, A1, A2, . . .) modes and the number of these modes depends on the product of the excitation frequency and the element thickness. For example, up to about 2 MHz·mm, only the two fundamental Lamb wave modes S0 and A0 will propagate in an Aluminum alloy plate.

Table 1. Characteristic phase velocities and wave lengths in a 1mm thick aluminium plate.

Frequency	Phase velocity [mm/μs]			Wavelength [mm]		
[kHz]	SH0	A0	S0	SH0	A0	S0
100	3182	964	5496	31.82	9.64	54.96
150	3182	1161	5495	21.21	7.74	36.63
200	3182	1318	5494	15.91	6.59	27.47
250	3182	1450	5492	12.73	5.80	21.97
300	3182	1564	5490	10.61	5.21	18.30

A characteristic feature of this type of wave motion is elliptical particles motion in contrast to Rayleigh (surface) waves, where the wave motion is circular.

The solution of the Lamb wave equations must be obtained numerically. As a result, dispersion relations for various Lamb wave modes are obtained, i.e. the dependence of the wave number on the frequencythickness product.
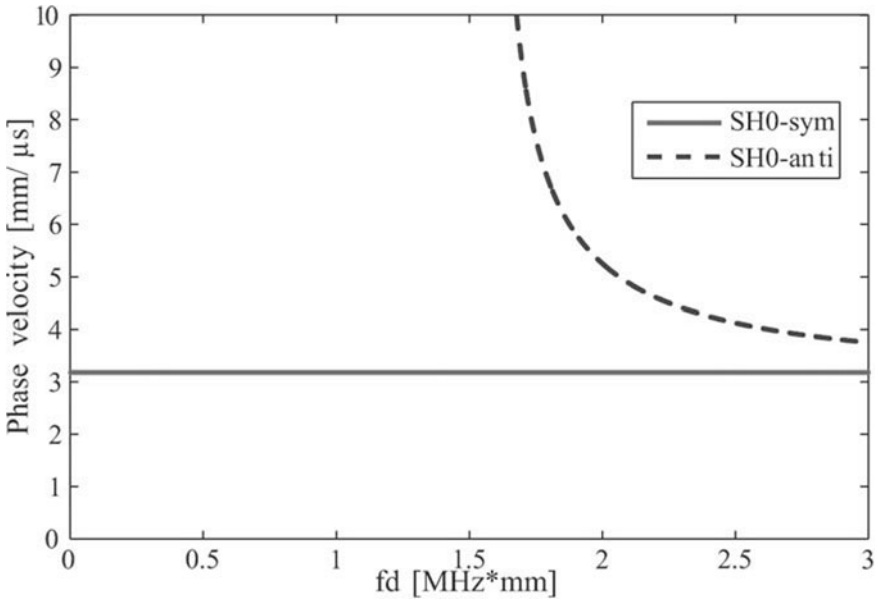
Figure 1. Phase velocity dispersion curves for an aluminium plate - shear horizontal waves.

It is interesting to look at the phase and group velocities of Lamb wave modes as well as shear modes corresponding to shear deformation. Typical results obtained for the group and phase velocity dispersion curves for the shear wave modes and the Lamb wave modes are presented in Figs. 1–4. These curves have been calculated analytically and obtained for an aluminium plate with the material properties as follows: Young's modulus 72.7 GPa, Poisson's ratio 0.33, mass density 2700 kg/m^3.

It can be noticed that in the frequency range up to around 2 MHz, only the fundamental modes can propagate in the plate. Some characteristic wave velocities and wave lengths in the case of the Aluminium plate under consideration are given in Table 1. The wave lengths are calculated from a simple equation,

$$\Lambda = \frac{c_{min}}{f} \tag{1}$$

where c_{min} is the minimal phase velocity and f denotes the carrier frequency of a wave packet. It can be noticed that the A0 mode has much shorter wavelengths in the lower frequency range than the SH0 and S0 modes; this means that A0 mode is well-suited to the detection of damage of rather small
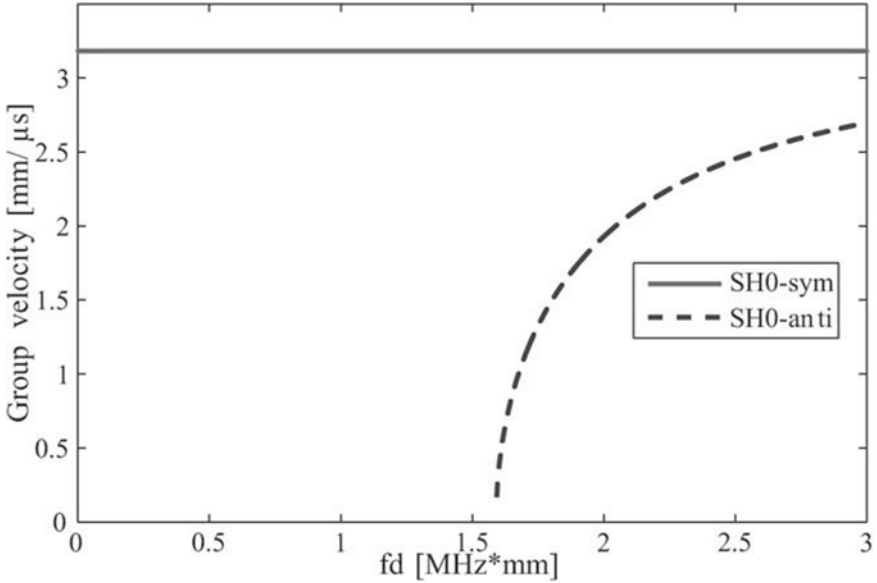
Figure 2. Group velocity dispersion curves for an aluminium plate - shear horizontal waves.

dimensions. In the case of the S0 and SH0 modes much higher frequency must be used in order to achieve comparable damage sensitivity. In contrast, the S0 mode is much less dispersive than A0 mode, while at the same time SH0 mode is almost *nondispersive* over all frequencies. (The term nondispersive means that a wave packet propagates in a structure without any observable distortion in shape.

Lamb waves propagating in a bounded solid media can be modelled assuming an appropriate displacement field, which in a accurate manner modes paths of particle motion through the thickness of the media. The displacement field can be approximated by,

$$
\begin{aligned}
u(x,y,z) &= \underline{u_0(x,y)} + \varphi_x(x,y) \cdot z + \underline{\psi_x(x,y) \cdot z^2} + \chi_x(x,y) \cdot z^3 \ldots \\
v(x,y,z) &= \underline{v_0(x,y)} + \varphi_y(x,y) \cdot z + \underline{\psi_y(x,y) \cdot z^2} + \chi_y(x,y) \cdot z^3 \ldots \quad (2) \\
w(x,y,z) &= w_0(x,y) + \underline{\varphi_z(x,y) \cdot z} + \psi_z(x,y) \cdot z^2 + \underline{\chi_z(x,y) \cdot z^3} \ldots
\end{aligned}
$$

where u_0, v_0 and w_0 represent the displacement components of the points located on a certain midplane surface, while φ_x and φ_y physically denote the rotations of appropriate solid sections about the x and y axes respectively. It is worth noting that the odd-order terms with respect to z in
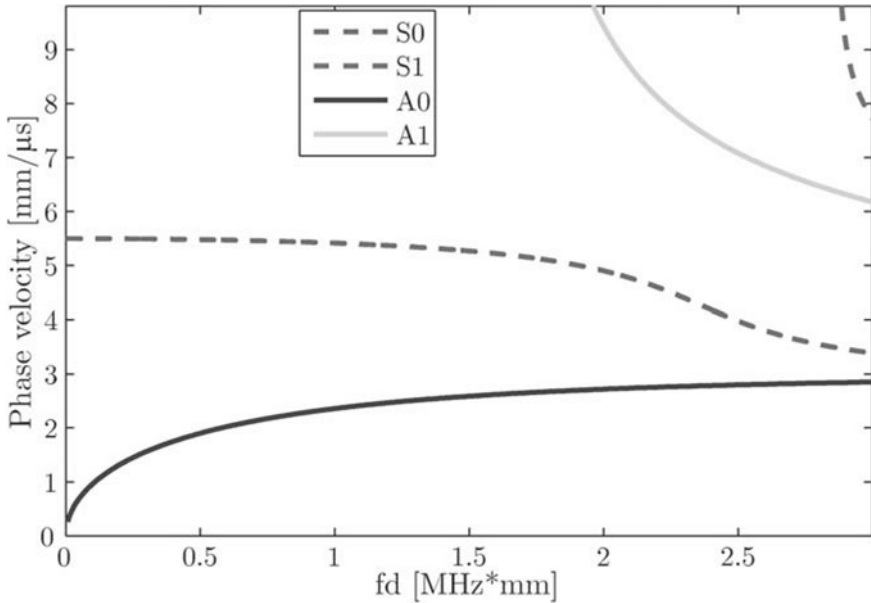
Figure 3. Phase velocity dispersion curves for an aluminium plate - symmetric and antisymmetric modes.

the x and y displacements together with the even-order terms in w with respect to z describe the antisymmetric wave modes and the other terms depict symmetric wave modes. Structural Health Monitoring (SHM) systems are usually based on the use of the fundamental modes of Lamb waves (S0 and A0), because in those cases it is usually much easier and convenient to analyse the received signals. An adequate approximation of the A0 mode requires at least the linear terms with respect to z in the u and v displacements and a constant term in the w displacement; this is consistent with the assumption of *First-Order Shear Deformation Theory* for plates. However, in order to capture the dispersion effect of the S0 mode, some additional terms must be included in the displacement field. It should be emphasised that application of the first-order shear deformation theory for plates in the case of spectral finite elements results in a diagonal form of the mass matrix for isotropic materials or symmetric laminates. In contrast, application of higher-order theories leads to generation of nonzero offdiagonal elements in the mass matrix; this means that the equations of motion are solved with much lower efficiency.
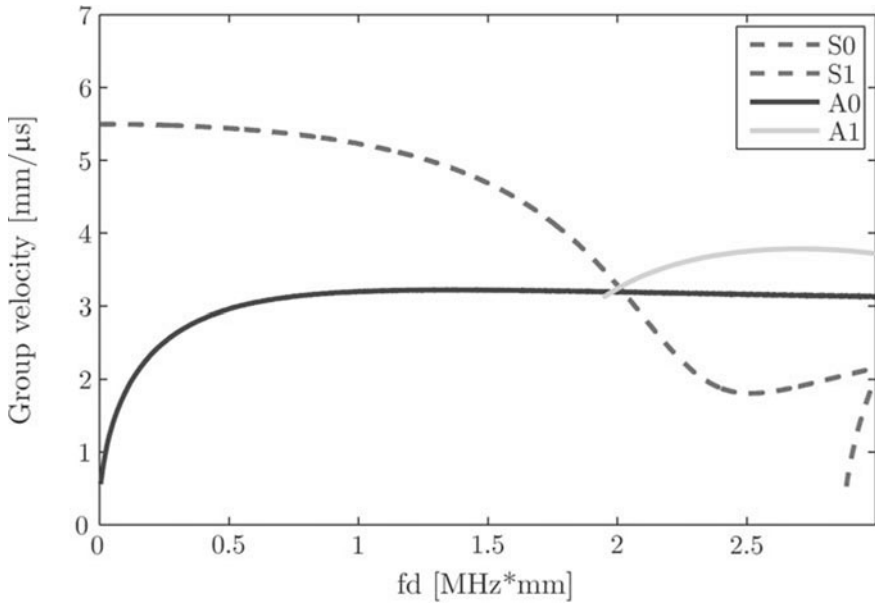
Figure 4. Group velocity dispersion curves for an aluminium plate - symmetric and antisymmetric modes.

4 Modelling of Elastic Waves

Wave propagation in structural elements has been studied over a considerable period of time. Although mathematical frameworks are well established and developed, wave propagation in real scale engineering structures still remains an open area of research. For simulation of stress wave propagation, the best way is to give an exact solution. However, even in some simple cases, such as elastic media, if local inhomogeneities (joints, inclusions, holes, etc.) are included, it is difficult to obtain exact solutions. For a specific geometry and finite periodic or semi-infinite boundary conditions, many solution techniques have been proposed and reported so far an excellent overview of theses techniques is given in (Bond, 1990).

In the case of SHM systems, piezoelectric actuators generate impulse wave signals and usually these are various modes of Lamb waves. The main problems in the analysis of high frequency (50 to 350 kHz) elastic wave propagation in structures with high velocities (1 to 6 km/s), are related to spatial discretisation. In order to obtain an accurate solution of the equation of motion, and to capture the effect of wave scattering at boundaries

and structural discontinuities, a huge number of degrees of freedom (dof) is
necessary. Conventional modal methods, when extended to high-frequency
regimes, become computationally inefficient since many higher modes that
should participate in the motion are misrepresented. For this reason, appli-
cation of some approximation method is necessary.

Among many methods used for modelling and studying the phenomena
of propagation of elastic waves, many numerical methods can be distin-
guished including: the finite difference method (FDM) (Strickwerda, 1989),
the finite element method(FEM) (Yamawaki and Saito, 1992; Koshiba et al.,
1984; Verdict et al., 1992; Alleyne and Cawley, 1992) and the boundary el-
ement method (BEM) (Cho and Rose, 1996). Unfortunately, the first two
methods are not only time–consuming, but also require large computational
memory even in the case of simple two–dimensional (2D) wave propagation
problems. Moreover, they suffer from *numerical dispersion* which leads
to improper wave velocity or false waves, which do not exist in the exact
solution. In contrast, the boundary element method (BEM) is less time–
consuming but application of the method to complex media with inhomo-
geneities is problematic.

Other methods are the finite strip element method (FSEM) and the
semi–numerical method (SNM)(Cheung, 1976; Liu and Xi, 2002; Liu et al.,
1990), which require much less memory storage space for necessary data due
to a lower level of discretisation and application of the exact solution in one
direction. SNM is very effective for the computation of forced wave motion
in the frequency domain and can be used for much higher frequencies than
the methods based on FEM. As with the BEM, the FSEM uses a Green's
function but in a different manner. On the other hand, variable size of
strip stiffness matrices and modification of spline functions at the boundary
nodes are inconvenient in implementation.

A method that incorporates the advantages of FEM (discretisation)
and the FDM (time integration schemes) is the unstructured grid method
(UGM) (Liu et al., 2004, 2005). This method is based on the dynamic equi-
librium equations of computational cells formed around auxiliary triangular
grids. The solution is obtained by the calculation of nodal displacements and
central point stresses of spatial grids alternately. A different approach has
been proposed by Schechter et al. (1994) and extended by Yim and Sohn
(2000). In the mass–spring–lattice–model (MSLM), inertia and stiffness
properties are calculated using lumped parameters. More recent develop-
ments in this area include the new Local Interaction Simulation Approach
(LISA) (Delsanto et al., 1992, 1994, 1997). This method simulates wave
propagation heuristically, i.e. directly from physical phenomena and prop-
erties. It should be noted that the LISA approach suffers from inaccuracy

in some cases (Ruffino and Delsanto, 1999).

More recently, various spectral methods have been proposed for the analysis of elastic wave propagation in complex media: the fast Fourier transform–based spectral finite element method (FFT–based SFEM) (Doyle, 1997) and the spectral element method (SEM) (Patera, 1984) also called the pseudospectral method. It should be stressed that despite the terminology, which may be misleading, these methods are completely different.

The FFT-based SFEM proposed by Doyle (1997) is very similar to the technique of the FEM as far as the assembly and the solution of the equation of motion is considered. The formulation of this method starts from exact solutions of the governing partial differential equations in the frequency domain. Excitation signals are transformed into a number of frequency components using the FFT. Next, as a part of a large frequency loop, the dynamic stiffness matrix is generated, transformed, and a solution is found for each unit impulse at each frequency. This yields directly the frequency response function (FRF) of the analysed problem. The calculated frequency domain responses are then transformed back to the time domain using the inverse fast Fourier transformation (IFFT).

The FFT–based SFEM proposed by Doyle is computationally efficient but the inverse Fourier transform is very difficult to do in an exact analytical manner. For this reason, many approximate and asymptotic schemes have usually been resorted to (Amaratunga and Williams, 1995). Such approaches reduce the problems associated with "wrap around"[1] due to the assumed periodicity of solutions in the FFT–based SFEM and thus may result in a decreased number of points in the time window for the same problem (Mitra and Gopalakrishnan, 2006). Further, FFT-based SFEM cannot be used for finite-length undamped structures. For such cases, a semi-infinite element (*throw-off* element (Doyle, 1997)) is normally used to allow some leakage of response, which in turn amounts to adding artificial damping through the release of trapped energy.

Consequently, the FFT-based SFEM is well suited to simple 1D problems (Palacz and Krawczuk, 2002; Krawczuk et al., 2003; Mahapatra and Gopalakrishnan, 2003), but becomes difficult to use for complex geometries. A comparative study of the FFT-based SEM with the LISA approach can be found in Lee et al. (2004). Despite problems with the periodic nature of the FFT, recent work in this area shows some application of the FFT-based SFEM to wave propagation phenomena in anisotropic plates and inhomogeneous layered media (Chakraborty and Gopalakrishnan, 2004, 2005,

---

[1]The "wrap around" effect means that the remaining part of the response beyond the chosen time window will start appearing first, which totally distorts the signal.

2006a,b).

The SEM, as proposed by Patera (1984), is much more versatile for the investigation of the propagation of elastic waves in structures of complex geometry. This method originates from the use of spectral series for the solution of partial differential equations (Boyd, 1989). The idea of the SEM is very similar to the FEM except for the specific approximation functions it uses. Elemental interpolation nodes are located at points corresponding to zeros of an appropriate family of orthogonal polynomials (Legendre or Chebyshev). A set of local shape functions consisting of Lagrange polynomials, which are spanned on these points, is built and used. As a consequence of this, as well as the use of the Gauss-Lobatto-Legendre integration rule, a diagonal form of the mass matrix is obtained. In this way, the cost of the time domain integration is much less expensive than in the case of the classic FE approach. Moreover, the numerical errors decrease faster than any power of $1/p$ (so-called *spectral convergence*), where p is the order of the applied polynomial (Pozrikidis, 2005). The main fields of application of SEM nowadays include fluid dynamics (Canuto et al., 1991), heat transfer (Spall, 1995), acoustics (Dauksher and Emery, 1997; Seriani, 1997), seismology (Komatitsch and Vilotte, 1998; Seriani, 1999), etc.

The application of SEM for problems of propagating waves in anisotropic crystals has been shown by Komatitsch et al. (2000).

The first attempt to use SEM for problems of propagation of elastic waves in 2D structural elements with cracks has been made by Żak et al. (2006). A 36-node spectral membrane element with two degrees of freedom per node has been developed. The crack has been modelled by simple splitting of the nodes between appropriate spectral elements. This approach has been extended to isotropic and composite plates (Żak et al., 2006; Kudela et al., 2007b,a). Also, the SEM found applications for the problems of wave propagation in anisotropic and inhomogeneous uncracked and cracked beams (Sridhar et al., 2006) as well as for the problems of cracked composite rods based on the three–mode theory of rods (Kudela and Ostachowicz, 2007).

A 3D spectral element has been developed and used for SHM purposes by (Kim et al., 2008).

It seems that the SEM is a most versatile and promising tool for wave propagation modelling and is becoming more and more popular in this field.
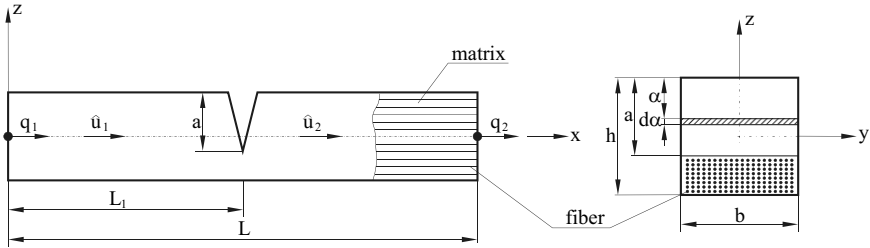
Figure 5. Composite spectral rod element.

4.1 The FFT–Based Spectral Finite Element Method – Cracked Rod

A multilayer composite spectral rod element is presented in Fig. 5. The crack is located at a distance of L_1 from the left hand end. The element has two nodes and one degree of freedom per node (longitudinal displacement). Nodal spectral displacements for the left and right parts of the rod are assumed as follows,

$$\hat{u}_1(x) = A_1 e^{-ik_n x} + B_1 e^{-ik_n(L_1-x)}, \quad x \in (0, L_1) \tag{3}$$

$$\hat{u}_2(x) = A_2 e^{-ik_n(x+L_1)} + B_2 e^{-ik_n[L-(L_1+x)]}, \quad x \in (0, L-L_1) \tag{4}$$

where the wave number is obtained from the equation,

$$k_n = \omega_n \sqrt{\frac{\mu}{D}} \tag{5}$$

The mass density per unit length can be expressed as,

$$\mu = \rho\, b\, h, \quad \mu = I_0 \tag{6}$$

for the isotropic and anisotropic cases, respectively. The material stiffness matrix has the forms,

$$D = E\, b\, h, \quad D = A_{11}\, b \tag{7}$$

for the isotropic and anisotropic cases, respectively. The mass density per unit length from Eq. (6) in the case of a composite rod can be expressed as,

$$I_0 = b \sum_{k=1}^{N} \rho_k \, (h_{k-1} - h_k) \tag{8}$$

where N is the number of composite layers, ρ_k is the mass density of the k-th layer and b is the rod width. The material stiffness matrix from Eq. (7) in the case of a composite rod can be expressed as (Vinson and Sierakowski, 1989),

$$D^e = b \sum_{k=1}^{N} (\overline{Q}_{11})_k \, (h_{k-1} - h_k)$$

$$\overline{Q}_{11} = E_{11} \sin^4 \theta + 2(\nu_{12} E_{22} + 2 G_{12}) \sin^2 \theta \cos^2 \theta + E_{22} \sin^4 \theta$$

(9)

where E_{11} is the Young's modulus along the reinforcing fibres, E_{22} is the Young's modulus in the direction perpendicular to the direction of the fibres, ν_{12} is the Poisson ratio, G_{12} is the shear modulus and θ is the angle between the material axis parallel to the reinforcing fibres and the x axis.

The coefficients A_1, B_1, A_2 and B_2 can be calculated as functions of the nodal spectral displacements using the following boundary conditions,

- at the left end of the element,

$$\hat{u}_1(0) = q_1 \tag{10}$$

- at the crack location (total change of displacements and compatibility of shear forces),

$$\hat{u}_2(0) - \hat{u}_1(L_1) = \hat{\theta} \frac{\partial \hat{u}_1(L_1)}{\partial x} \tag{11}$$

$$\frac{\partial \hat{u}_1(L_1)}{\partial x} = \frac{\partial \hat{u}_2(0)}{\partial x} \tag{12}$$

- at the right end of the element:

$$\hat{u}_2(L - L_1) = q_2 \tag{13}$$

where $\hat{\theta} = Ebhc$ and c is the flexibility at the crack location (see section 4.3). Taking into account the formulae describing nodal spectral displacements for the left and right parts of the element, the boundary conditions can be written in a matrix form as,

$$\begin{bmatrix} A_1 \\ B_1 \\ A_2 \\ B_2 \end{bmatrix} = \mathbf{W}^{-1} \begin{bmatrix} q_1 \\ 0 \\ 0 \\ q_2 \end{bmatrix} \tag{14}$$

$$\mathbf{W} = \begin{bmatrix} 1 & e^{-ik_n L_1} & 0 & 0 \\ (ik_n\hat{\theta} - 1)e^{-ik_n L_1} & -1 - ik_n\hat{\theta} & e^{-ik_n L_1} & e^{-ik_n(L-L_1)} \\ -ik_n e^{-ik_n L_1} & ik_n & ik_n e^{-ik_n L_1} & -ik_n e^{-ik_n(L-L_1)} \\ 0 & 0 & e^{-ik_n L} & 1 \end{bmatrix}$$

(15)

The nodal spectral forces can be determined by differentiating the spectral displacements with respect to x, and then can be expressed as follows,

$$\hat{F}_1 = D\frac{\partial \hat{u}_1(0)}{\partial x}$$

(16)

$$\hat{F}_2 = D\frac{\partial \hat{u}_2(L - L_1)}{\partial x}$$

(17)

The relation between nodal displacements and forces can be shown as,

$$\begin{bmatrix} \hat{F}_1 \\ \hat{F}_2 \end{bmatrix} = \mathbf{K_d} \begin{bmatrix} \hat{q}_1 \\ \hat{q}_2 \end{bmatrix}$$

(18)

where the dynamic stiffness matrix is given by,

$$\mathbf{K_d} = D \begin{bmatrix} ik_n & -ik_n e^{-ik_n L_1} & 0 & 0 \\ 0 & 0 & -ik_n e^{-ik_n L} & ik_n \end{bmatrix} \mathbf{W}^{-1}$$

(19)

Unlike conventional finite elements, a special case is derived here where the rod is very long and application of any load at any location causes no secondary disturbances other than incident waves departing from that location. This simulates a condition, wherein the boundaries are at such a distance that the effect of reflected waves becomes negligible due to attenuation throughout their long travel, and do not reach the location under consideration within the time of observation. In other words, the *throw–off* element is a non–resonant single–node element that acts as a conduit to allow the propagation of the trapped energy out of the system. The nodal spectral displacement for the throw–off element is assumed in the following form,

$$\hat{u}(x) = C_1 e^{-ik_n x} + D_1 e^{-ik_n(L_1-x)}, \quad x \in (0, L_1)$$

(20)

After using transformations similar to Eqs. $(10 - 19)$ the frequency dependent stiffness matrix $\mathbf{K_t}$ for the *throw–off* rod element can be defined as,

$$\mathbf{K_t} = Dik_n$$

(21)

4.2   The Time Domain Spectral Element Method – Cracked Rod

Spectral rod finite elements with crack, are formed by the connection of two classic spectral finite elements with nodes separated by the use of a spring. Spectral elements based on the elementary and three-mode theory are presented in Figure 6.
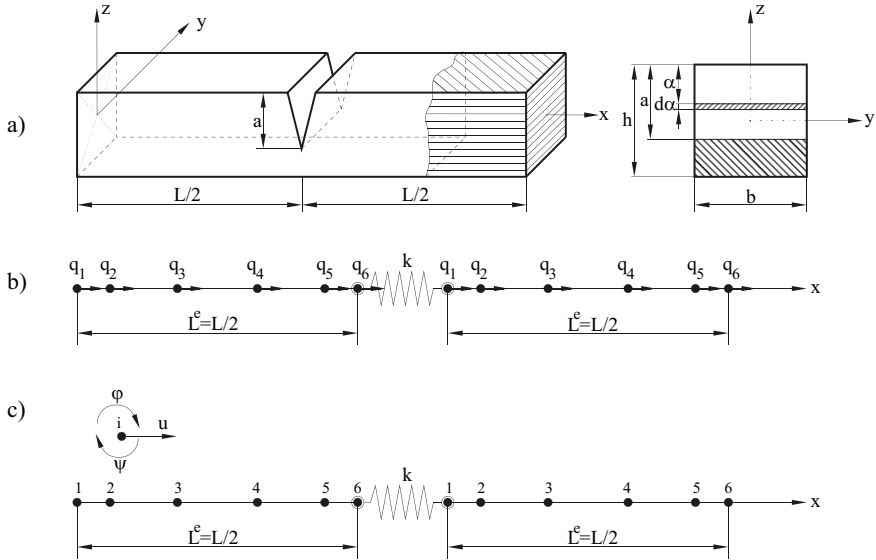
Figure 6. Schematic diagrams of models a) model of the composite rod fragment with crack, b) spectral finite element for the elementary theory, c) spectral finite element for the three–mode theory.

The stiffness of the spring modelling the size of a transverse, non-growing crack is calculated according to the laws of fracture mechanics. The effect of the crack is achieved at the stage of global stiffness matrix assembly.

The rod spectral finite element has been derived according to elementary theory; the element consists of 6 nodes. With each node, one degree of freedom is given, i.e. longitudinal displacement. Nodes are placed unequally. Local nodal coordinates $\xi_i \in [-1, 1]$, $i \in 1, \ldots, 6$ are obtained as roots of the equation,

$$\left(1 - \xi^2\right) P_5^{'}(\xi) = 0 \tag{22}$$

where $P_5^{'}(\xi)$ denotes the first derivative of Legendre's 5th-order polynomial. The obtained coordinates correspond to Gauss-Lobatto-Legendre integration points. On such selected points, Lagrange's approximation is defined

which gives a set of shape functions. The same set of shape functions can be used for displacement field approximation inside the element as well as for element geometry approximation. A spectral rod element applied to the modelling of a composite rod with crack derived according to the elementary theory of rods is presented in Figure 6a. The element contains 6 nodes; each node has one degree of freedom – longitudinal displacement. In the elementary theory of the rod, displacements take the following form,

$$u(x, z) = u_0(x) \tag{23}$$

where u_0 is the average axial displacement. The strain field may be expressed by the equation,

$$\varepsilon_x(x, z) = \frac{\partial u_0}{\partial x} \tag{24}$$

Assuming an approximation of the displacement field within the element,

$$u^e(\xi) = \mathbf{N}^e \mathbf{q}^e = \sum_{i=1}^{6} N_i^e(\xi) \, q^e(\xi_i) \tag{25}$$

where $\mathbf{N}^e$ are shape functions, and $\mathbf{q}^e$ are nodal degrees of freedom within the element, and substituting into equation (24), one obtains the strain approximation,

$$\varepsilon_x^e(\xi) = \mathbf{B}^e \mathbf{q}^e = \sum_{i=1}^{6} B_i^e(\xi) \, q^e(\xi_i) \tag{26}$$

where $\mathbf{B}^e$ is the matrix connecting strains with nodal displacements calculated as,

$$\mathbf{B}^e = \frac{\partial}{\partial x} \mathbf{N}^e(\xi), \quad \frac{\partial}{\partial x} = J^{-1} \frac{\partial}{\partial \xi}, \quad J = \frac{\partial x}{\partial \xi} \tag{27}$$

Matrices of mass and stiffness are calculated numerically with the use of the Gauss-Lobatto-Legendre integration rule,

$$\mathbf{m}^e = \int_{\Omega_e} \left[\mathbf{N}^e(x) \right]^T I_0^e \, \mathbf{N}^e(x) \, \mathrm{d}x \approx \sum_{i=1}^{6} w_i \left[\mathbf{N}^e(\xi_i) \right]^T I_0^e \, \mathbf{N}^e(\xi_i) \, \det(J^e) \tag{28}$$

$$\mathbf{k}^e = \int_{\Omega_e} \left[\mathbf{B}^e(x) \right]^T D^e \, \mathbf{B}^e(x) \, \mathrm{d}x \approx \sum_{i=1}^{6} w_i \left[\mathbf{B}^e(\xi_i) \right]^T D^e \, \mathbf{B}^e(\xi_i) \, \det(J^e) \tag{29}$$

Quadrature weights $w_i > 0$, that are independent of the element are estimated from the formula,

$$w_i = \frac{2}{n(n-1) \left[P_{n-1}(\xi_i) \right]^2}, \quad i \in 1, \ldots, n \tag{30}$$

where $n = 6$ for the 6–node element.

Time Domain Integration   For the sake of the accuracy of solution, discretisation of the area with the use of the spectral finite element method ought to provide at least 5 nodes per wave length[2]. Moreover, the mesh of the elements should be, if possible, homogeneous over the entire area. After spatial discretisation with spectral elements, to achieve a solution, only the following system of differential equations in the time domain is needed,

$$\mathbf{M\ddot{Q}} + \mathbf{KQ} = \mathbf{F} \tag{31}$$

where $\mathbf{M}$ is the global inertia (mass) matrix, $\mathbf{K}$ is the global stiffness matrix, $\mathbf{Q}$ is the vector of global degrees of freedom, and $\mathbf{F}$ is the vector of time dependent forces. Damping is omitted, as it is possible to consider wave attenuation based on experimental measurements.

Discretisation in the time domain of the system of differential equations of the second degree (31), may be conducted with the classic Newmark's scheme or the central difference scheme. The given methods are conditionally stable methods of direct integration, where the equation of the motion is integrated step by step; this means that the equation of motion (31) ought to be fulfilled only at chosen moments in time. For the stability of the solution (to avoid accumulation of integration errors and rounding errors) the integration step Δt must be adequately small. The calculation of an adequate integration step in the simulation of wave propagation within composite elements is difficult owing to the great number of parameters of the problem (minimum and maximum speed, carrier wave frequency, time of analysis, and number of nodes per wavelength). In practice, in the application of the central difference method, the number of integration steps should be chosen individually for the considered problem. It may be assumed that the integration step Δt is proportional to p^{-2}, where p denotes the order of the approximating polynomial in the spectral element. This means that a high degree of polynomial leads to a significant cost of calculation. In the case of too small a number of integration steps, the algorithm is unstable and this manifests itself in a violent increase of the displacements with each time step.

It should be emphasised that in the method of spectral elements, spatial discretisation is very accurate, owing to the fact that it is based on high–order polynomials. On the contrary, in the case of time domain discretisation with the use of a central difference scheme only second–degree accuracy is obtained, which means that global accuracy is reduced. For this

---

[2]For 5th-order approximating polynomials

reason, application of a higher–order scheme in the time domain would be interesting.

In the method of central differences, one assumes changeability of the acceleration vectors in time in the form of:

$$\ddot{\mathbf{Q}} \simeq \frac{1}{\Delta t^2}\left(\mathbf{u}_{t+\Delta t} - 2\,\mathbf{u}_t + \mathbf{u}_{t-\Delta t}\right) \tag{32}$$

Substituting the difference formula (32) into equation (31) and marking the displacement vector at time t as $\mathbf{u}_t = \mathbf{Q}$, one obtains,

$$\frac{1}{\Delta t^2}\left(\mathbf{u}_{t+\Delta t} - 2\,\mathbf{u}_t + \mathbf{u}_{t-\Delta t}\right)\mathbf{M} + \mathbf{K}\mathbf{u}_t = \mathbf{F}_t \tag{33}$$

From equation (33) one calculates the sought displacement condition at the time step $t + \Delta t$, meaning $\mathbf{u}_{t+\Delta t}$. This is obtained based on the solution at time t. For this reason, this method is numbered among *explicit* methods. The great advantage of this manner of solving equation (31) is the fact that the matrix of stiffness does not have to be inverted.

One should draw attention to the fact that calculation of the results at the current time step, using results obtained at the previous time step, requires assuming a certain starting procedure. One assumes that the vectors $\mathbf{Q}_0$, $\dot{\mathbf{Q}}_0$, $\ddot{\mathbf{Q}}_0$ are known at the initial time, namely at the time $t = 0$. This way, using the difference formula for the second derivative (32) and a difference formula for the first derivative,

$$\dot{\mathbf{Q}} \simeq \frac{\mathbf{u}_{t+\Delta t} - \mathbf{u}_{t-\Delta t}}{2\Delta t} \tag{34}$$

one can calculate the displacement vector $\mathbf{u}_{t-\Delta t}$ at a fictional moment, which will precede the beginning of the motion,

$$\mathbf{u}_{t-\Delta t} = \mathbf{Q}_0 - \Delta t\dot{\mathbf{Q}}_0 + \frac{\Delta t^2}{2}\,\ddot{\mathbf{Q}}_0 \tag{35}$$

Frontal method   Despite using various formats to store sparse matrices, which provides saving of the computer's RAM, wave issues are so complex that the computer's memory resources are usually not sufficient. It is possible, in some cases, to use the frontal method, in which algebraic equations of a matrix are calculated at the level of the finite element without the necessity to formulate global matrices.

(Kudela, 2008) proposed an integration method for the wave equations, where assembly of the global stiffness matrix does not take place. The algorithm of the method is presented below.

After ordering, equation (33) takes the form,

$$\underbrace{\left(\frac{1}{\Delta t^2}\mathbf{M}\right)}_{\mathbf{M}_0}\mathbf{u}_{t+\Delta t} = \mathbf{F}_t - \underbrace{\mathbf{K}\mathbf{u}_t}_{\hat{\mathbf{F}}} + \underbrace{\left(\frac{1}{\Delta t^2}\mathbf{M}\right)}_{\mathbf{M}_0}\mathbf{u}_t - \underbrace{\left(\frac{2}{\Delta t^2}\mathbf{M}\right)}_{\mathbf{M}_2}\mathbf{u}_{t-\Delta t} \quad (36)$$

In the equation (36), the vector $\hat{\mathbf{F}}$ may be calculated in such a manner that the use of the global stiffness matrix $\mathbf{K}$ is not necessary. The proposed explicit time integration algorithm has the following steps:

- Loop over elements e
  - For each element calculate the characteristic elemental matrices $\mathbf{k}^e$, $\mathbf{m}^e$
  - Assemble each diagonal mass matrix of the element e into the global vector $\mathbf{M} = \overset{n_{el}}{\underset{e=1}{\mathrm{A}}}\mathrm{diag}\,(\mathbf{m}^e)$, where $\overset{n_{el}}{\underset{e=1}{\mathrm{A}}}$ denotes the assembly operator
  - Successive elemental stiffness matrices $\mathbf{k}^e$ can be stored in a binary file
- End of loop over elements e
- Define constants $a_0 = 1/\Delta t^2$, $a_2 = 2a_0$
- Calculate the auxiliary vectors $\mathbf{M}_0 = a_0\,\mathbf{M}$, $\mathbf{M}_2 = a_2\,\mathbf{M}$, $\tilde{\mathbf{M}}^\alpha = 1/\mathbf{M}_0^\alpha$
- The displacement vector $\mathbf{u}_{t-\Delta t}$ is calculated from Eq. (35)
- Apply the initial conditions at the time instant $t = t_0$
- Loop over time instants t
  - Set up a pointer to the elemental stiffness matrix $\mathbf{k}^e$ at the beginning of the file
  - Loop over elements e
    * Read the stiffness matrix $\mathbf{k}^e$ from the file and move the pointer
    * Perform multiplication $\hat{\mathbf{f}} = \mathbf{k}^e\mathbf{u}_t^I$, where I denotes the vector with numbers of degrees of freedom corresponding to element e
    * Assemble vector $\hat{\mathbf{F}} = \overset{n_{el}}{\underset{e=1}{\mathrm{A}}}\left(\hat{\mathbf{f}}^e\right)$
  - End of loop over elements e
  - Calculate effective vector $\tilde{\mathbf{R}} = \mathbf{F}_t - \hat{\mathbf{F}} + \mathbf{M}_0^\alpha\mathbf{u}_t^\alpha - \mathbf{M}_2^\alpha\mathbf{u}_{t-\Delta t}^\alpha$, where indices α denote that multiplication is performed element by element without summation
  - The solution of the equation of motion at the time instant $t + \Delta t$ is achieved by multiplication of element by element: $\mathbf{u}_{t+\Delta t}^\alpha = \tilde{\mathbf{M}}^\alpha\tilde{\mathbf{R}}^\alpha$

− $\mathbf{u}_{t-\Delta t} = \mathbf{u}_t$, $\mathbf{u}_t = \mathbf{u}_{t+\Delta t}$, $t = t + \Delta t$

• End of loop over time instants t

The proposed integration algorithm of the wave equation provides optimal use of computer memory resources - the global stiffness matrix is not assembled; this enables the solving of problems with a great number of degrees of freedom on an ordinary PC. The proposed algorithm is extremely efficient since it uses the diagonal form of the mass matrix so that inversion of the matrix is completely eliminated.

4.3 Flexibility at the crack location

The flexibility at the crack location for a spectral rod element can be calculated using the Castigliano theorem (Przemieniecki, 1968):

$$c_{ij} = \frac{\partial^2 U}{\partial S_i \partial S_j} \quad \text{(for } i = j = 1\text{)} \tag{37}$$

where U denotes the elastic strain energy of the element caused by the presence of the crack and the S_i are the independent nodal forces acting on the element. The following relation can express the elastic strain energy due to the crack,

$$U = \frac{1}{E} \int_A K_I^2 \, \mathrm{d}A \tag{38}$$

where A denotes the area of the crack and K_I is a stress intensity factor corresponding to the first mode of the crack formation (Tada et al., 1973). The stress intensity factor can be expressed as follows,

$$K_I = \frac{S_1}{bh} \sqrt{\pi \alpha} \, f\left(\frac{\alpha}{h}\right) \tag{39}$$

where α, b and h denote the crack depth, height of the rod and width of the rod at the crack location respectively (see Fig. 6), and f is the correction function in the form (Tada et al., 1973),

$$f\left(\frac{\alpha}{h}\right) = \sqrt{\frac{\tan(\pi\alpha/2h)}{\pi\alpha/2h}} \, \frac{0.752 + 2.02(\alpha/h) + 0.37[1 - \sin(\pi\alpha/2h)]^3}{\cos(\pi\alpha/2h)} \tag{40}$$

After some simple transformations, the flexibility of the elastic element, which is used for modeling the cracked cross section of the rod, can be rewritten as,

$$c = \frac{2\pi}{\overline{E}b} \int_0^{\overline{a}} \overline{\alpha} \, f^2(\overline{\alpha}) \, \mathrm{d}\overline{a} \tag{41}$$

where $\overline{E}$ denotes Young's modulus (averaged with respect to any layers of composite).

It should be noted that application of the technique of static node condensation as presented in section 4.1 in the case of SEM, causes the mass matrix to lose diagonality. In order to maintain the diagonal form of the mass matrix it is necessary to split nodes between two spectral elements and add to the global stiffness matrix a special matrix. This special matrix is a consequence of the inverse form of the flexibility at the crack location and can be expressed as follows:

$$\mathbf{K_s} = \begin{bmatrix} 1/c & -1/c \\ -1/c & 1/c \end{bmatrix} \tag{42}$$

In such a case, the mass matrix of the elements located next to the crack is identical with that of classical spectral elements.

4.4   Comparative example

Numerical calculations were conducted for an unconstrained rod with dimensions: length 2 m, height 0.02 m and width 0.02 m. The following properties of materials were assumed: Young's modulus 210 GPa and mass density 7860 kg/m^3. Excitation, in the form of an impulsive force with amplitude 100 N was applied to the node on the left end of a rod. A forcing signal in the form of a sine with five cycles, modulated with a Hanning window, was applied.

The aim of the numerical example is to compare results obtained by the use of the spectral element method with the spectral element method based on FFT (Palacz and Krawczuk, 2002). In this example, the applied forcing signal had a carrier frequency of 100 kHz. However, for signal amplitudes to be compared, the excitation amplitude for the second method is twice as large. Such a procedure is necessary because in the method based on the FFT, on the left end of the rod an element of the *throw-off* type is added. This causes the actuated wave to propagate simultaneously in two directions: to the left it is led *ad infinitum* by the *throw-off* element, and to the right it propagates because of the element with the crack. The crack was inserted exactly in the centre of the rod. It was assumed that the depth of the crack was 15% of the height of the rod.

Figures 7–9 present comparisons of the signals obtained by the use of both methods. For legibility, the distance covered by the wave was placed on the horizontal axis. Distance was obtained by calibration of the time axis with the theoretical velocity $v = \sqrt{E/\rho} = 5168.9$ m/s. In addition, the beginning of the excitation was shifted adequately to half of the impulse time.
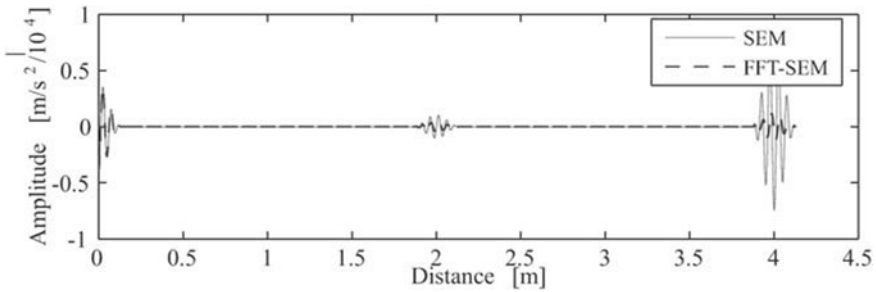
Figure 7. Comparison of signals on the left end of the rod, obtained with the method of spectral elements (SEM) and the method of spectral elements based on the FFT (FFT-SEM).
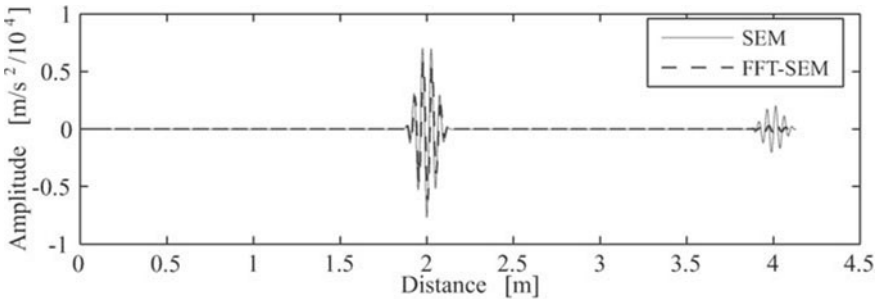
Figure 8. Comparison of signals on the right end of the rod, obtained with the method of spectral elements (SEM) and the method of spectral elements based on the FFT (FFT-SEM).

In Figure 7 one can observe that for both methods, the wave velocity corresponds to the theoretical velocity - the centre of the impulse occurs almost precisely at the distance of 2 m, i.e. once the wave covers the distance from the left end of the crack and back to the left end. The next centre of the impulse occurs at the distance equal to 4 m and it corresponds to the reflection from the right end of the rod. In both methods the shape of the signal remains the same, whereas amplitudes differ.

Taking into account the fact that issues of wave propagation in a medium without damping are discussed, the signal amplitude value should not undergo changes. This is the case only when the method of spectral elements is applied, as is presented in Figures 7-8, where the impulse amplitudes at the distance of 4 m (Figure 7) and 2 m (Figure 8) are identical. For the
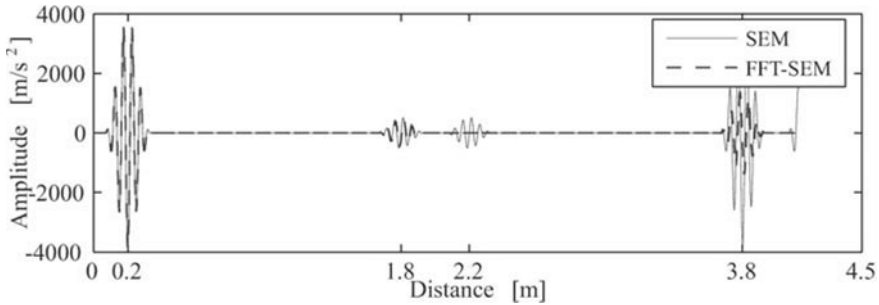
Figure 9. Comparison of signals in the point located 20 cm from the left end of the rod, obtained with the method of spectral elements (SEM) and the method of spectral elements based on the FFT (FFT-SEM).

spectral element method based on FFT, the signal amplitude decreases as a result of energy transfer from the system through the *throw-off* element.

Influence of the *throw-off* element on the signal received at the a location of 20 cm from the left end of the rod is presented in Fig. 9. The wave generated at the left end of the rod, while propagating, travels through discussed location (impulse at the distance of 0.2 m), it reflects from the crack and returns to this location (impulse at the distance of 1.8 m), next it reaches the left end of the rod, where the wave is transferred ad infinitum without reflection from the edge (no impulse at the distance of 2.2 m).

The comparative analysis allows one to state that the method of spectral elements shows a certain advantage over the FFT-based spectral elements method in the fidelity of modelling the phenomenon of wave propagation. When only the first reflection (from the crack) is analyzed, the considered methods lead to compatible results. The only condition is, that in the FFT-based spectral element method, the analyzed location will not agree with the degree of freedom where the *throw-off* was added. The advantage of the FFT-based spectral element method is that if one searches for solutions only at several locations, the time of calculation is shorter. Continuing the theoretical deliberation, the numerical examples presented will be based on the spectral element method.

Attention should be brought to the fact that the formalism presented in paragraphs 4.3-4.1 refers to the elementary theory of rods. However, expanding this formalism to other theories of rods, beams or plates is straightforward. From the point of view of SHM, the elementary theory of rods is not sufficient at higher frequency ranges because it does not take into account the dispersive character of the waves. The above aspect is clearly

presented in Fig.10, where comparison of signals received in a composite rod with a crack modelled using elementary and three-mode theory was presented. Signals received by the use of the model based on elementary
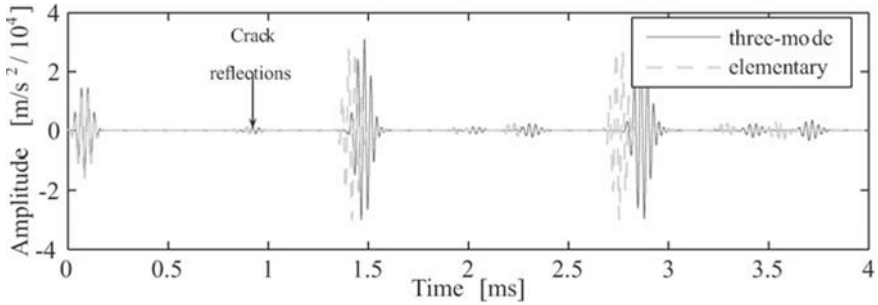
(a) Signal with carrier frequency 30 kHz.
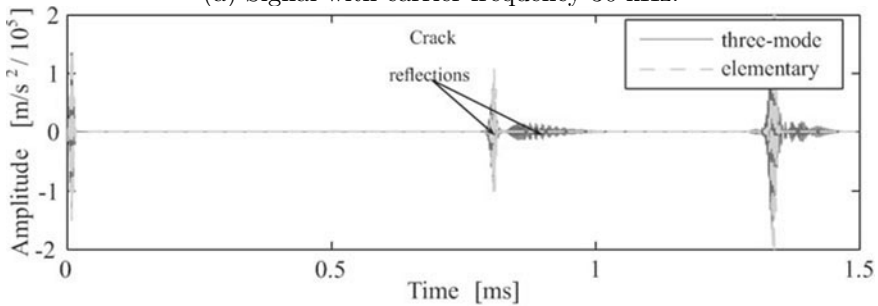
(b) Signal with carrier frequency 300 kHz.

Figure 10. Comparison of the signals received on the left end of the rod with crack at the depth of 15% of section height for the tree-mode and elementary theory.

theory, significantly differ from signals received with the use of the model based on three-mode theory, in regard to both wave velocity and shape of signal packet.

4.5   Influence of crack on wave propagation

Influence of crack location and crack depth on wave propagation
Figure 11 presents the absolute values of signals obtained at the left end of the rod for various locations of a crack with 15% of the cross-section height. Location of the crack close to the left end of the rod causes multiple reflections and superpositions of waves. With the location of the crack at a shorter distance from the half–length of the rod (Figure 11), one can observe
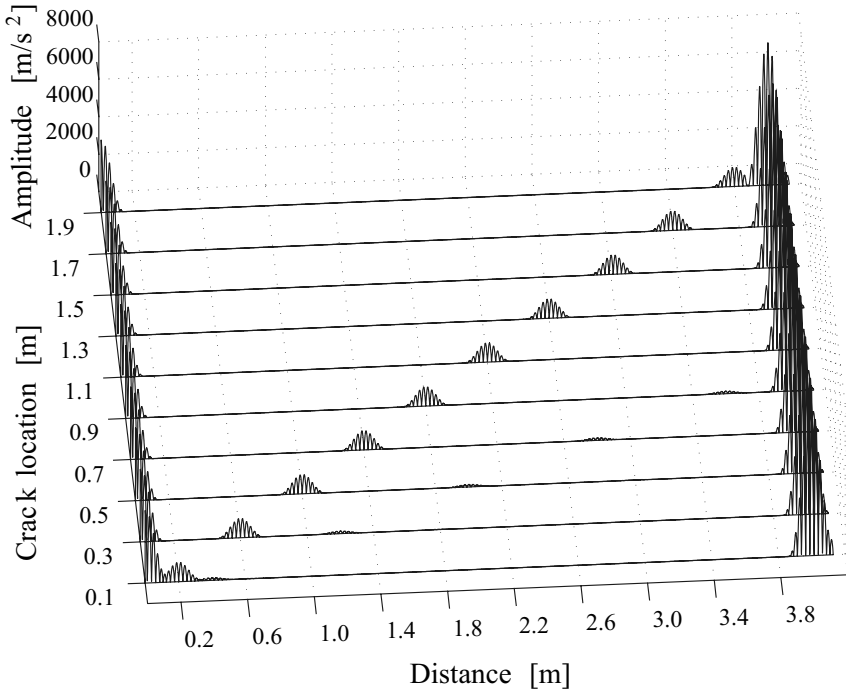
Figure 11. Influence of crack location at the depth of 15% of cross–section height, on wave propagation.

two reflections from the crack and a reflection from the right end of the rod. The example presented shows that the location of the crack may be easily identified based on the time of flight and the velocity of the wave packet.

In the next example, the effect of depth of the crack was studied. The crack was located at a distance of 1.2 m from the left end of the rod. With an increase in crack size, the amplitude of the signal reflected from the crack increases, and the amplitude of the signal passing through the crack decreases, as presented in Figure 12. For a crack depth of 5% of the cross-section height, the wave impulse reflected from the crack also occurs, although this is not very visible in Figure 12

Influence of signal frequency on amplitude of the reflected wave
It follows from Figure 13 that along with an increase of forcing signal frequency, there is increased amplitude of the signal reflected from the crack
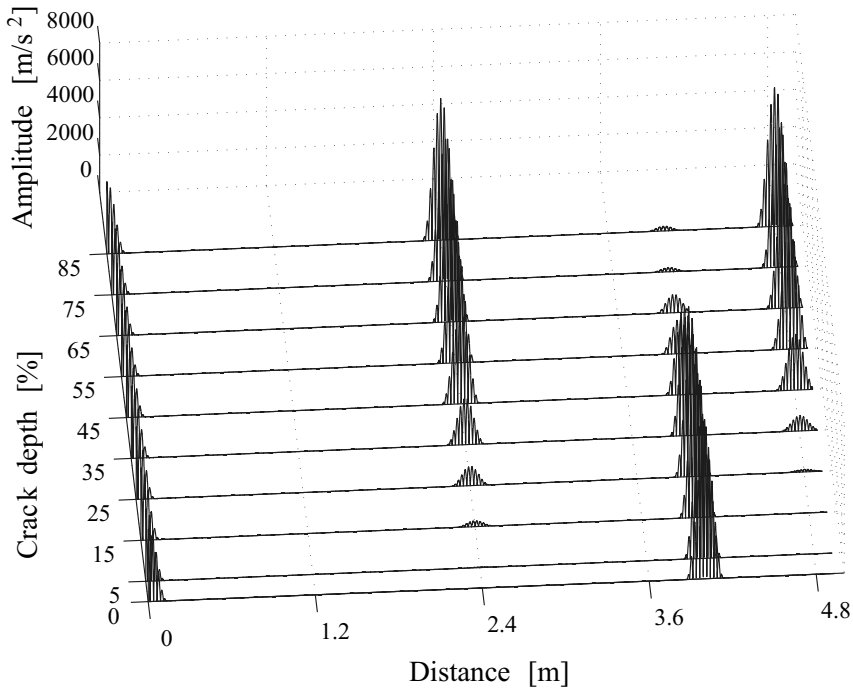
Figure 12. Influence of the crack depth, situated at the distance of 1.2 m from the left end of the rod, on wave propagation.

in relation to the amplitude of the signal received at the place of excitation. This means that sensitivity of damage detection methods based on changes in elastic wave propagation will be higher for higher frequency ranges. However, one must take into account the fact that, in reality one deals with elastic waves whose velocity depends on frequency, and therefore the signal undergoes dispersion. In order to take into consideration the above effect, one must apply Love's theory, Mindlin–Hermann's theory or three-mode theories, depending on the frequency range (Krawczuk et al., 2004).

5 Damage Identification in 1D Structures

Damage identification problems may be treated as inverse problems, but it is also possible to do damage identification based on knowledge in the field of wave propagation. In the former case, a high-fidelity numerical model of the analysed structure is necessary. Moreover, reference signals (signals
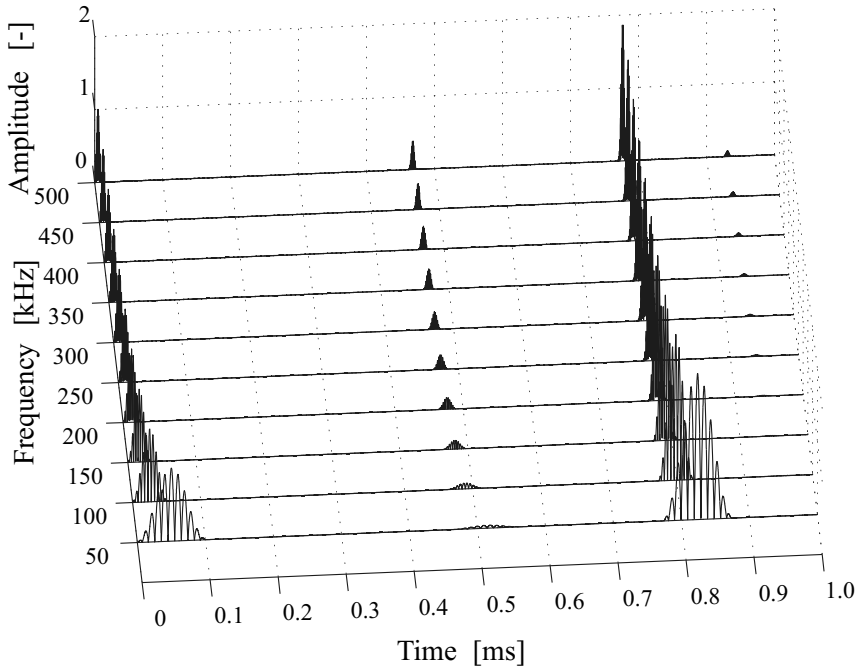
Figure 13. Signal frequency impact, on propagation of the wave reflected from a crack with the size of 15% of section height.

received for non-damaged structures) theoretically are not necessary. But in practice higher signal-to-noise ratio is obtained using differential signals. In the latter case, identification of damage may take place by processing the signals registered at sensors embedded in real objects. Monitoring of the structure in real-time is also possible because calculation time is very short in comparison with the former case. The use of reference signals means that better damage identification results can be obtained. Aspects of the application of both techniques, are illustrated by the example of the rod in Figure 14.

It was assumed that the geometry of the rod, material properties, and signal parameters were the same as in the comparative analysis of section 4.4. The rod was divided into 255 spectral elements. Damage of a size of 15% of the section height, at a distance of $L_c = 60.16$ cm from the left end of the rod, was inserted into the model. Simulation of experimental measurements was conducted, assuming an arbitrary distribution of two
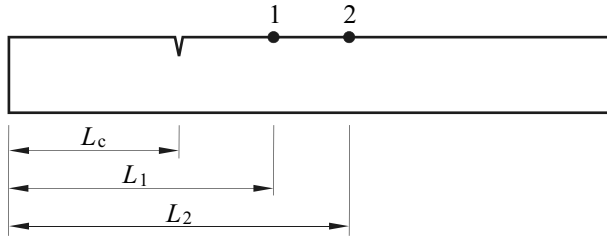
Figure 14. Schematic diagram of the rod with crack and sensors.

"PZT transducers" at distances of $L_1 = 89.84$ cm and $L_2 = 110.16$ cm. It was also assumed that each of the transducers could also work as a wave actuator and as a sensor at the same time. In this way, 4 signals were obtained. These were next contaminated by random noise with a quantity not exceeding 3% of the maximum amplitude of the signal. A similar simulation was conducted for the non–damaged rod.

Detection   Because signals coming from real measurements contain noise, it should be minimised by filtering and the level of noise ought to be estimated. Giving an estimate of noise level is difficult in automation. The level of the noise may be estimated by making several measurements from the same sensors and conducting a statistical analysis. After performing an operation of subtraction on two signals registered in various operating conditions one will obtain the noise. If within the structure there is enough damage that there is the difference between signals, one will observe exceedance of the noise level (Fig. 15a). Unfortunately in this way, damages for which the amplitude of the reflected wave is lower than the noise level, will not be detected (Figure 15b). To overcome these obstacles, two methods of extracting features connected with damage from the signals could be proposed. The objective of these methods is to to get a smooth function with improved signal-to-noise ratio.

Method I   The first method is simple weighted summation of signal amplitudes in a moving window (a type of cross-correlation) according to the equation,

$$e(t_j) = \sum_{i=1}^{N_w} \left[F(t_i) \, S \left(t_j + (i-1)\Delta t \right) \right]^2 \qquad (43)$$

where S is the processed signal, F is a weight function, which may be a window modulating the signal (e.g. a Hanning window or a Gaussian

window), Δt denotes the time step, N_w is the number of points in the moving window (in practice $N_w = t_e/\Delta t$, where t_e stands for the excitation time).

Method II The second method is a similar weighted summation, but corresponding to the power spectrum,

$$e(t_j) = |\mathcal{F}(f_c)| \approx |\mathrm{DFT}\left[F(t_i)\, S\left(t_j + (i-1)\Delta t\right)\right]|, \quad i = 1, \ldots, N_w \quad (44)$$

where $\mathcal{F}$ denotes the linearly interpolated amplitude corresponding to the carrier frequency of the excited signal f_c, DFT denotes the discrete Fourier transform. To clarify, e is named as the *intensity function of reflected waves* because this function gives peaks corresponding to the location of reflected wave packets.

Application of the above–mentioned techniques regarding the signal presented in Figure 15b and alteration of the time scale causes amplification of the function e at the location of wave reflections (after transformation the signal is shorter by the width of moving window), which is presented in Figure 16. Method II introduces signal operations in the time domain as well as in frequency; this enables signal filtration to be more favourable than in the case of method I. In Figure 16 one can observe, that in method II the relation of the maximum value of the *intensity function of reflected waves* to the estimated noise level is much higher than in the case of method I.

In the literature many other methods of feature extraction can be found (wavelet analysis, pattern recognition, outlier analysis, etc.).

Localisation Estimation of the propagation time is a basis for adequate location of the damage. Techniques of time propagation estimation, based on the maximal signal envelope created using the Hilbert transform, may be unreliable if the level of noise in the signal is too high. Instead of the signal envelope, one may use, as suggested in section 5, the *intensity function of reflected waves*.

Estimation of the propagation time may be conducted on the signal received at the sensor number 2, when excitation occurs in transducer number 1 (t_{1-2}) and inversely (t_{2-1}). From the experimental simulation one obtains adequately $t_{1-2} = t_{2-1} = 0.0393$ ms, which gives, with the distance between sensors $L_2 - L_1 = 20.32$ cm, a propagation velocity of 5166 m/s, almost identical to the theoretically calculated velocity. Those values were obtained through application of the above-mentioned methods I and II. The time of propagation, calculated with the use of the envelope and Hilbert
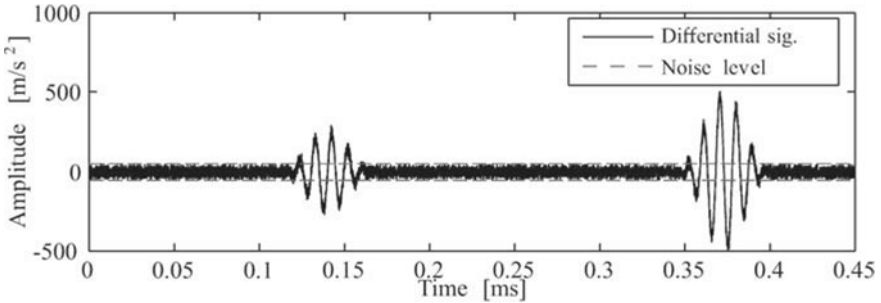
(a) Crack with a size of 15% of the height of the rod.
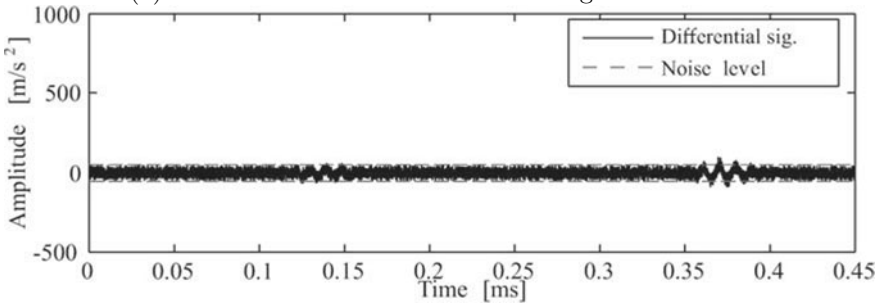
(b) Crack with a size of 5% of the height of the rod.

Figure 15. Difference in signals between non-damaged rod and rod with crack against estimated noise level background.

transform, adequately shows $t_{1-2} = 0.0391$ ms and $t_{2-1} = 0.0395$ ms. Such a discrepancy shows the lower precision of estimation.

Knowing the velocity of wave propagation and the location of the sensors, the *intensity function of reflected waves* can be transformed from the time domain to the distance domain in such a way that suitable superpositions of reflected waves occur,

$$E(x_j) = \sum_{i=1}^{N_S} e_i \left(t(x_j) \right), \qquad t(x_j) = \frac{d_{Tx}^j + d_{xS}^j}{c} \qquad (45)$$

$$d_{Tx}^j = \sqrt{(x_j - x_T)^2}, \qquad d_{xS}^j = \sqrt{(x_j - x_S)^2} \qquad (46)$$

where x_j is the presently considered rod coordinate, x_T stands for the excitation coordinate, x_S stands for the sensor coordinate, N_S denotes the total number of sensors, and c is the estimated velocity of wave propagation.
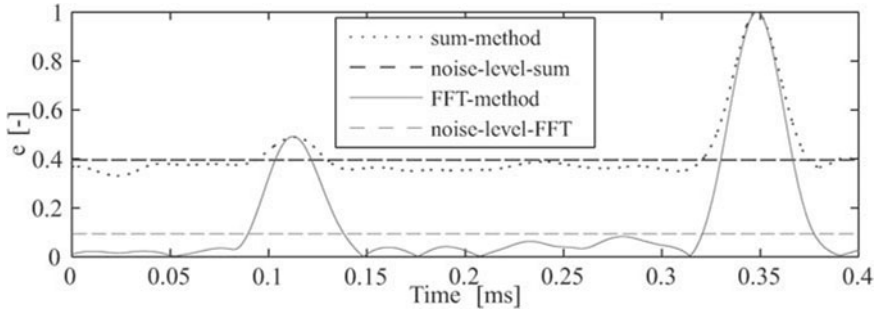
Figure 16. Differential signal filtered with the use of methods I and II, against estimated noise level background.
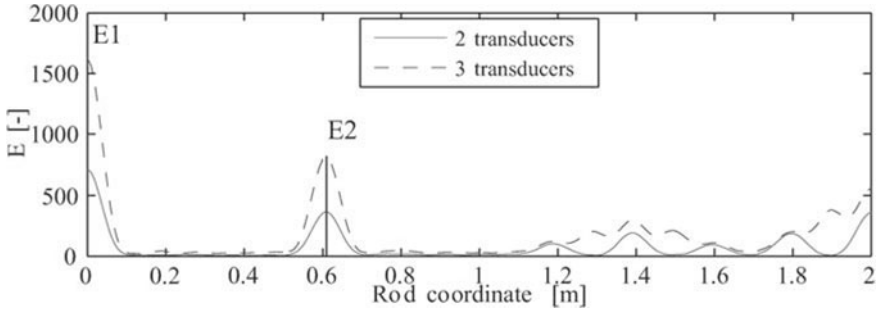
Figure 17. Amplification *intensity function of reflected waves* with application of two and three sensors.

The procedure presented in equations (45)-(46) was applied for the sensor configuration given in Figure 14 and for a configuration with additional sensors located between sensors number 1 and number 2. As a result, the amplified *intensity functions of reflected waves* presented in Fig. 17 were obtained. Amplification of the wave reflected from the crack occurs about 0.6 m from the left end of the rod (amplitude E_2). However, the wave reflected from the edge of the rod is also amplified (amplitude E_1). It can be observed, that the amplification is connected with the number of sensors and is equal to $E/e = N_s^2$.

Estimation of the damage size The size of the damage may be estimated by taking into account the relation of the amplitude of the wave reflected from the damage A_R with the amplitude of the excited wave A_T.

Because of the noise in the signal, the amplitudes A_R and A_T may be replaced with the amplitudes of the *intensity functions of reflected waves* e_R and e_T. However, it is necessary to familiarise oneself with the relation of e_R/e_T to crack depth. Such a relation may be defined in the process of experimental research or based on a numerical model (Fig. 18).
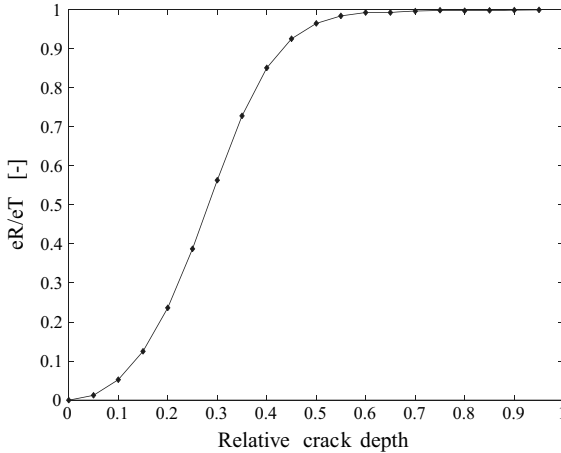
Figure 18. Relative crack influence on relation e_R/e_T with carrier frequency 100 kHz (numerical model).

Attention should be brought to the fact that, for very small cracks, it is difficult to calculate the amplitudes e_R from signals containing noise. Therefore, it is easier to calculate the relation e_R/e_T indirectly. Assuming amplitude symbols according to Figure 17 for the case with three sensors, one obtains $E_2 = 818.0$. Applying the procedures given in equation (44) for signals registered for a rod without damage, one obtains the amplitude of the *intensity function of reflected waves* directly at the location of excitation $e_{ref} = 728.25$. The relation e_R/e_T may be expressed by the equation,

$$\frac{e_R}{e_T} = \frac{E_2/N_s^2}{e_{ref}} \qquad (47)$$

In the analysed example, $e_R/e_T = 0.1248$, and with the reference to the relation presented in Fig. 18, corresponds to a crack with a depth of 15% of the height in cross–section of the rod.

Genetic algorithms in the problem of identification Genetic algorithms are extremely suitable for the problem of optimisation of func-

tions with multiple minima (maxima) or discontinuous functions (Goldberg, 1989). The genetic algorithm (GA) differs substantially from more traditional search and optimisation methods. The four most significant differences are:

- GAs search a population of points in parallel, not a single point.
- GAs do not require derivative information or other auxiliary knowledge; only the objective function and corresponding fitness levels influence the directions of search.
- GAs use probabilistic transition rules, not deterministic ones.
- GAs work on an encoding of the parameter set rather than the parameter set itself.

Those features predestine genetic algorithms to applications in problems regarding damage identification.

It is important to note that the GA provides a number of potential solutions to a given problem and the choice of final solution is left to the user. In cases where a particular problem does not have one individual solution (for example the solution is a family of crack locations) as in the case of multi-objective optimisation and scheduling problems, then the GA is potentially useful for identifying these alternative solutions simultaneously (Chipperfield et al., 1994).

Having the signals from the simulated experiment and numerical model of the rod presented in Section 4.2, an attempt was made to identify the location and size of the damage simultaneously. It was assumed that both decision variables, location of the crack m and depth of the crack n, would be encrypted in one chromosome divided into two parts,

$$\underbrace{1\ 0\ 0\ 1\ 0}_{m}\ \underbrace{0\ 1\ 1\ 1}_{n}$$

The decision variables are represented by integers, ranging over $[0, 2^p - 1]$, where p denotes the number of bits in the chromosome. This enables easy modelling of the damage, because the locations agree with nodes of the mesh of the spectral finite elements. What is more, the following data were assumed:

- number of individuals 40,
- maximum number of generations 20,
- crossover probability 0.7,
- mutation probability 1/40,

The objective function, which is to be minimised, was suggested in the form of,

$$f(m,n) = \sum_{i=1}^{N} \sum_{j=1}^{4} |(R_{ij} - S_{ij}(m,n))| \tag{48}$$

where N denotes the number of points in the registered signal, R_{ij} stands for the j-th amplitude of the i-th signal from the simulated experiment, and $S(m, n)$ are the signal amplitudes obtained by using the numerical model, with the parameters specified by the decision variables m and n. The signals $S(m, n)$ are continuously calculated, because the number of possible locations and sizes of the crack may be relatively large (depending on the precision of the calculation). To shorten the calculation time, the problem was solved in two stages.

Stage I   In this stage a 9-bit chromosome was assumed, where 5 bits fall to the decision variable m, and 4 bits fall to decision variable n. This assumption corresponds with ranges of representation, $m \in [0, 31]$ and $n \in [0, 15]$, when $m = 0$ and $n = 0$ denote that damage does not occur, and the remaining whole numbers correspond to positions of the crack location and size given by the number of divisions (Figure 19). In this way the crack cannot occur at the distance equal to 0 as well as equal the length of the rod, and the size of the crack cannot reach 100% of the cross–section height.
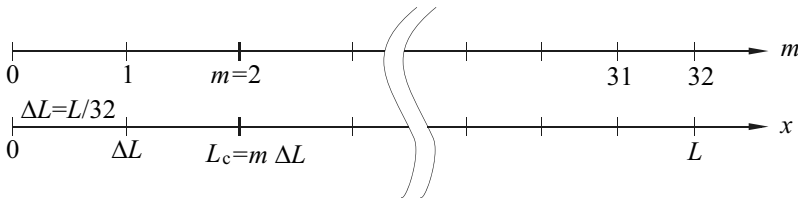
Figure 19. Schematic diagram of rod division in stage I.

In the analysed example, the genetic algorithm already converges to a result after two generations: $m^I = 10$, $n^I = 2$; this refers to a coordinate of crack location $L_c^I = 0.625$ and a size of crack $a^I = 0.125$. This solution is the first approximation, which is the starting point to stage II.

Stage II   In this stage an 8-bit chromosome is assumed, where 4 bits fall to the decision variables m and n. The solution is searched for within a range situated to the left and to the right of the approximation found in stage I, thus,

$$L_c \in \big[(m^I - 1) \, \Delta L^I, \; (m^I + 1) \, \Delta L^I \big)$$

and similarly for the size of the crack a. The division resulting from the assumption of a four-bit representation of the decision variables, is presented

in Figure 20. This time, the decision variables $m = 0$ and $n = 0$ correspond to the left ends of the ranges.
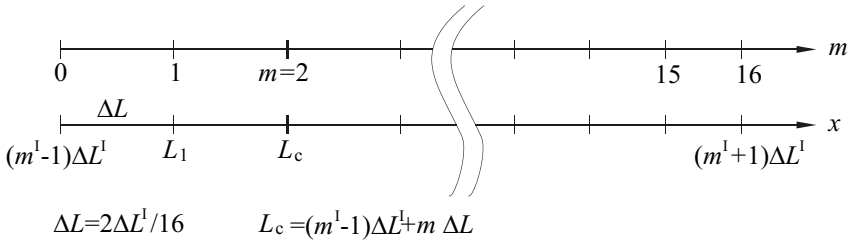
Figure 20. Schematic diagram of rod division in stage II.

In this example, after six generations the genetic algorithm gives a solution: $m^{II} = 5$, $n^{II} = 11$; this corresponds to coordinates of the crack location $L_c^I = 0.6016$ m and the size of the crack $a^{II} = 0.1484$. The obtained solution is exact as far as the location of the crack is concerned - this results from the assumed discretisation (255 elements, between which one may model the crack), and shows about 0.2% deviation as far as the depth of the crack is concerned.

Conclusions   To summarise, the conception of a damage identification system based on knowledge of the field of wave propagation as well as the conception based on genetic algorithms, leads to considerable results. In both cases, the location and size of the damage were identified with high precision. On the other hand, the identification of damage in two–dimensional elements of a structure based on genetic algorithms may be too complex for contemporary computers.

6   Experimental Applications of Lamb Waves

6.1   Test stand profile

The test stand in the Department of Mechanics of Intelligent Structures in The Institute of Fluid-Flow Machinery of the Polish Academy of Sciences consists of piezoelectric transducers, measuring devices designed for wave generation and data acquisition, and a computer (Fig. 21). The measuring device is a prototype device, constantly developed and improved. In general, the device is superb for the needs of wave propagation analyses. An electronic system enables registration of signals from 12 measuring channels, while the 13th channel is used for wave generation. The device may

be connected to the computer through a USB connector in order to control its parameters and transfer measured signals.
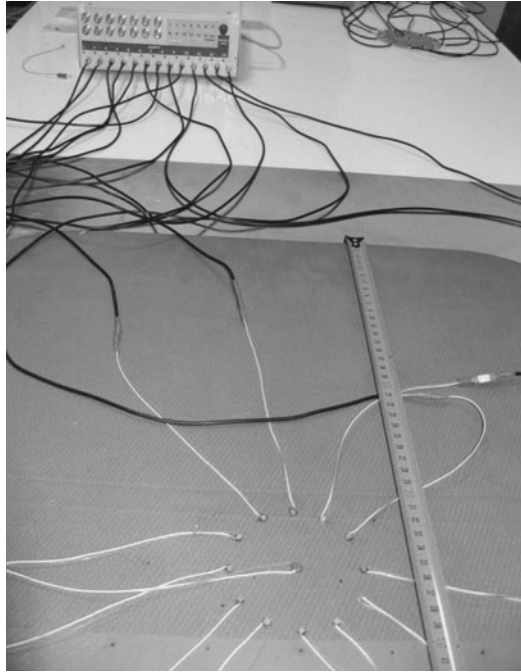
Figure 21. View of the fragment of a test stand.

The configuration of the matrix of piezoelectric transducers is in the shape of a clock with transducers placed on each "hour" of the round "clock face" and an additional transducer which is placed in the centre of the transducer configuration (Fig. 22). Elastic waves are generated by means of a central piezoelectric transducer CMAP11 (5 mm x 5 mm x 2 mm) or CMAP10 (3 mm x 3 mm x 2 mm) made by Noliac. Wave registration takes place at circumferential transducers CMAP10 (3 mm x 3 mm x 2 mm) also made by Noliac. However, it is also possible to generate the waves in the circumferential transducers. The limitation of the device is that the transducer generating the elastic waves cannot operate at the same time as the sensor registering the elastic waves.

The subject of research here is a composite panel, whose shape and dimensions are given in Figure 22. It is a part of a door from an Agusta AW-139 helicopter. The panel is made of six layers of carbon-epoxy laminate
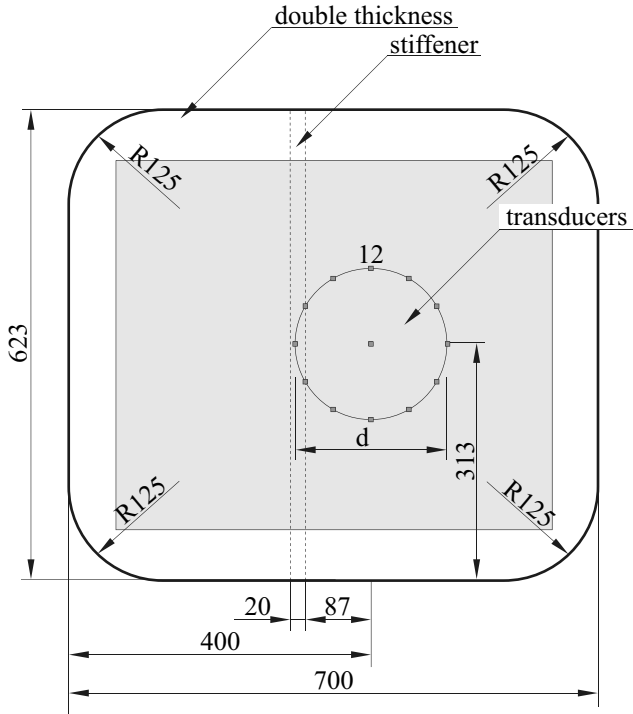
Figure 22. Geometry of the sample and distribution of sensors.

with the ply stacking sequence [+45/-45/0/90/+45/-45], and covered with a sealing compound with a thickness of about 0.14 mm, which makes up the face board of the door. The theoretical total thickness of the composite plate is equal to about 1.15 mm.

Transducers were attached to the studied specimen using a wax substance, the same that is used in assembling accelerometers. This enables easy assembly and non-destructive disassembly of transducers, which is important owing to the lowered costs of the experimental research. Connecting transducers to the surface of a structure using wax is a relatively cheap solution and at the same time practical. However, it is not an optimal solution because the wax strongly attenuates elastic waves and what is more, precise bonding of transducers is difficult. In practical monitoring systems, one should apply durable bonding e.g. using epoxy resin with mechanical properties similar to the surface, to which transducers are attached. The influence of the bonding layer thickness and its Young's modulus, on the glued

Table 2. Properties of materials (Żak et al., 2000; com)

	Sealing compound	Epoxy resin	Carbon fibre
Youngs Module, GPa	3.43	3.43	230
Poissons coefficient	0.35	0.35	0.2
Density, kg/m^3	1350	1250	1750

connection of the piezoelectric element, was studied in the work by Qing et al. (2006). Experimental results indicate that increasing the glue thickness changes the electromechanical impedance, the resonance frequency of piezoelectric element and the amplitude of the signal registered by the sensor. The influence of Young's modulus of the bonding layer on the signal amplitude is insignificant.

6.2   Theoretical dispersion curves

Because the mechanical properties of the specimen are unknown, for theoretical calculations the data given in the Table 2 were assumed. These values are verified according to group velocity profiles measured by experiment. With the use of a procedure described in work by Kudela et al. (2007b), dispersion curves were calculated (i.e. the group velocity dependence on frequency). It should be emphasised that this procedure was extended in a way that takes into account the asymmetrical ply stacking sequence and covering face lamina. Results are presented in Figure 23. Within the range of frequency around 1-600 kHz the longitudinal wave propagates the fastest (S0), next is the shear wave (SH0), and the slowest is the bending wave (A0). Above a frequency of about 600 kHz there occur other modes of Lamb waves.

Similarly, a group velocity distribution diagram was obtained depending on propagation angle (Figure 24) with frequency of 120 kHz. It is important that values of group velocities of the longitudinal wave (S0) and the shear wave (SH0) significantly differ from the average, i.e. the shape of the profile of group velocity significantly differs from a circle. The situation is different in the case of the bending wave (A0), where the mentioned differences are much smaller. Owing to this fact, in methods of damage localisation based on the time of flight of waves reflected from the damage, the most favourable modes for analysis are the bending waves. It is also important that in the analysed element of structure, the bending wave is characterised by minimal dispersion within the frequency range above 100 kHz (the course of the dispersion curve for the velocity of A0 mode for frequencies above 100 kHz in Figure 23 is similar to a horizontal line).
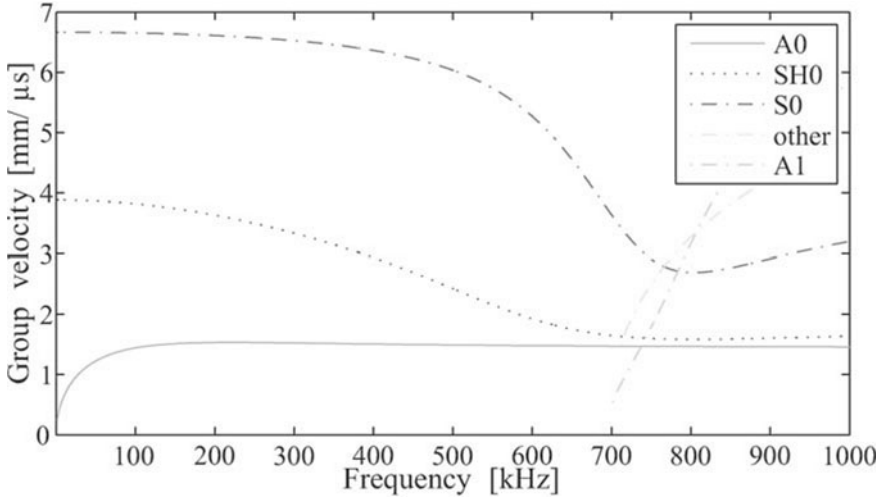
Figure 23. Theoretical dispersion curves obtained for the studied carbon-epoxy laminate.

6.3   Estimation and verification of wave group velocities

Measurements were conducted using a sinusoidal excitation modulated by a Hanning window within a frequency range of 50–150 kHz with a 10 kHz step. As a result of the modulation, signals with 3, 5, 7 and 10 cycles have been investigated. For the estimation of group velocity, a windowing method based on the signal spectrum energy was used. Selected results of the experiment are presented in Fig. 25.

Figure 25 presents the dependence of group velocities on the wave propagation direction, with given excitation frequencies for different number of cycles. Individual points are distributed with a 30 degree angle, corresponding to the distribution of sensors. Diagrams were also plotted with a dashed line, the theoretical curve of velocity profile for a composite with a fibre stacking sequence [+45/-45/0/90/+45/-45]. With frequencies above 100 kHz (the minimal dispersion area) the velocities estimated based on experimental signals almost agree regardless of the number of cycles, and their distribution depending on propagation angle to a large extent agrees with the theoretical profile. It should also be added that for a frequency range corresponding to the dispersion profile, velocities are the most similar to circles, which is beneficial in application to the methods of damage localisation.

A conclusion from this research is that, owing to high wave attenuation
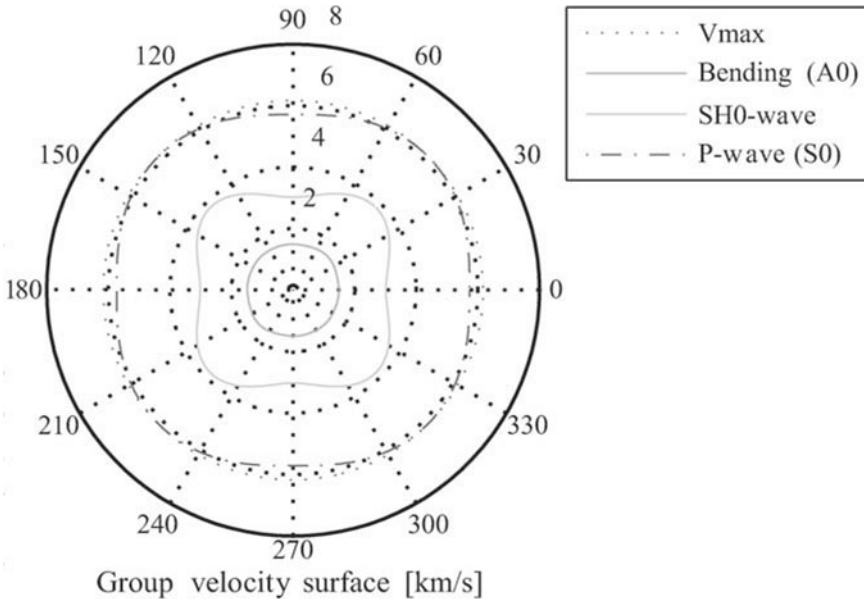
Figure 24. Theoretical graph of group velocity distribution depending on propagation angle, obtained for the studied laminate with a frequency of 120 kHz.

(due to composite material damping), inspection of a panel area is only possible within a radius of 0.5 m for a frequency of 50 kHz. With an increase of the frequency, wave attenuation also increases.

It should be emphasised that, in the registered signals, the predominant wave amplitudes are connected with bending waves. Shear and longitudinal waves are also present in the signals but their amplitudes are very small with reference to the amplitudes of the bending waves. For this reason, based on registered signals one cannot estimate the velocity of longitudinal and shear wave propagation. However, shear and longitudinal waves propagate with higher velocity than bending waves. Moreover, they undergo mode conversion, which causes additional signal disturbances.

6.4   Damage detection

Piezoelectric transducers were attached to the studied sample using wax. A "clock" configuration of sensors with a radius of about 4 cm was applied. A series of measurements for a non-damaged sample as well as for a sample
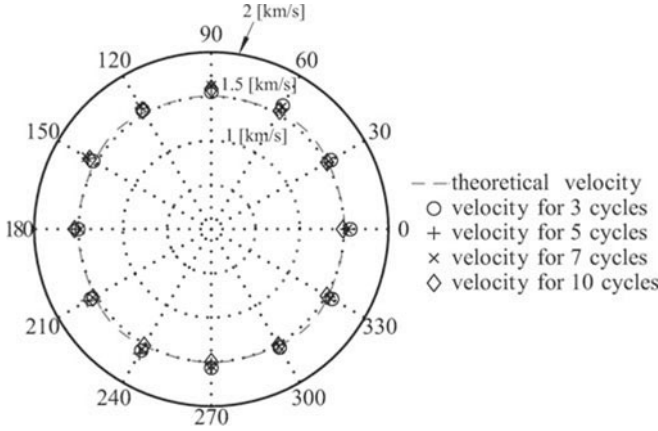
Figure 25. Group velocity dependence on the propagation angle with excitation frequency of 120 kHz for an even number of cycles.

with various artificially inserted damages were conducted. Signal processing was carried-out using an algorithm suggested by Kudela et al. (2008). The complicated geometry of the studied sample and the composite material with strong damping behaviour, of which the sample was made, mean that distinction between waves reflected from damage and reflected from features of the structure (edges, stiffener, depth change, etc.) is impossible. For this reason, it is necessary to use reference signals. That is why, after application of the signal processing procedure, the amplitudes of signals registered for the damaged sample s_r were linked to the amplitudes of signals registered for the non–damaged sample s_d using a dB scale:

$$E_{d-r} = 10 \log_{10} \left(\frac{E_d}{E_r} \right) \tag{49}$$

where E_d and E_r refer to superimposed *intensity functions of reflected waves* e_d and e_r given by Eq. (44) in the case of signals registered for the damaged (s_d) and reference (s_r) structure, respectively. The functions E_d and E_s in the case of 2D problems can be described by the formula:

$$E = \sum_k \int_S e_k(x,y)dS \approx \sum_k \sum_{i,j} e_k(x_i, y_j),$$

$$k = 1, \ldots, 12 \quad i = 1, \ldots, N \quad j = 1, \ldots, M \tag{50}$$

Table 3. Inserted cracks scenario

no	crack no 1		crack no 2	
	depth [mm]	length [mm]	depth [mm]	length [mm]
a	0.2	4	-	-
b	1	4	-	-
c	1	8	-	-
d	1	14	-	-
e	1	18	-	-
f	1	18	1	4
g	1	18	1	8
h	1	18	1	15

where S is the surface of the investigated structure, and N and M stand for the total number of nodes i and j, located on the surface of the investigated structure; k is the sensor number. This function gives a map which can be called a *damage influence map* or *damage intensity map*.

As an indicator of the damage level of the element of structure, a value described with the following formula was assumed:

$$D = \sum_{ij} |E_{d-r}(x_i, y_j)| \tag{51}$$

After a series of tests it was found that a frequency of about 120 kHz is the optimal frequency for signal excitation[3]. Further researches were conducted using only a frequency of excitation of 120 kHz.

6.5 Crack detection

Within the studied sample, cracks were inserted according to the scenario given in Table 3. As a result of the damage detection algorithm suggested in the work by Kudela et al. (2008), one finds maps of damage influence as presented in Figure 26. On the maps of damage influence, the real location of the crack for reference purposes was clearly marked with a white line.

While analyzing the maps of damage influence presented in Figures 26a–c one may notice an increase in the value of map amplitudes in the form of circumferential stripes, which the radius agrees with the radius where damage is located. By increasing the damage to a length of 8 mm, the map of damage influence (Figure 26c) reaches a maximal value in the close

---

[3]For a signal excitation frequency of 120 kHz the biggest differences were noted between signals in damaged and non-damaged sample, what manifested in the biggest values of damage level indicator D

neighbourhood of the damage (difference between centre of the crack and maximal value of damage influence map is equal to about 25 mm). Further increasing of the crack length brings about surprising results. Amplitudes of damage influence maps presented in Figures 26d–e undergo strengthening, not only in the place where the crack occurs but also in other areas. What is more, the maximal amplitude value of the damage influence map decreases with increase of the damage length. The observed anomalies may be explained by the effect of mode conversion. Shear and longitudinal waves converted from the bending mode propagate faster. Damage influence maps are made based on the bending wave velocity profile, therefore strengthening or attenuation of the amplitudes of the damage influence maps occur also in areas which do not agree with the location of the crack. What is more, a problem may be caused by noise (*coherent noise*) that results from inaccuracy in signal amplitude subtraction (in the dB scale of logarithmic relation between signal amplitudes), which for example are shifted at random against one another.

Insertion of the second crack causes significant changes in the damage influence maps (Figures 26f–h). One may observe that the maximal value of the damage influence maps increase along with the increase of the second crack's length. Despite the fact that the second crack is located closer to the sensor configuration, it is impossible to locate unambiguously the crack based on the damage influence map. One may only estimate the radius where the crack is located, and only in the case of the crack with a length over 10 mm (Figure 26h).

Despite difficulties in formulating a crack localisation method, experimentation in their detection proves to be relatively simple. Damage detection may occur based on the damage indicator values represented in formula (51). First, one must experimentally establish a threshold value which, once surpassed, will indicate damage of the structure. Figure 27 presents dependence of the damage level indicator on the damage scenarios put together in Table 3. Also, an arbitrary established threshold level of the value $1.75 \cdot 10^5$ was applied to the Figure 27. The damage level indicator takes a lower value than the threshold level only in the case of damage scenario "a", i.e. a crack within the face layer of the sample. Insertion of a crack with a depth of 1 mm into studied sample, causes exceedance of the threshold level. One may state that the indicator of damage level, shows an increasing tendency along with size and number of inserted cracks with the exception of damage scenario "d". This indicator may be effectively used for damage detection purposes in the early stage of development.

In the case of experimental research concerning delamination detection, the situation is similar to the case of matrix crack detection. However,
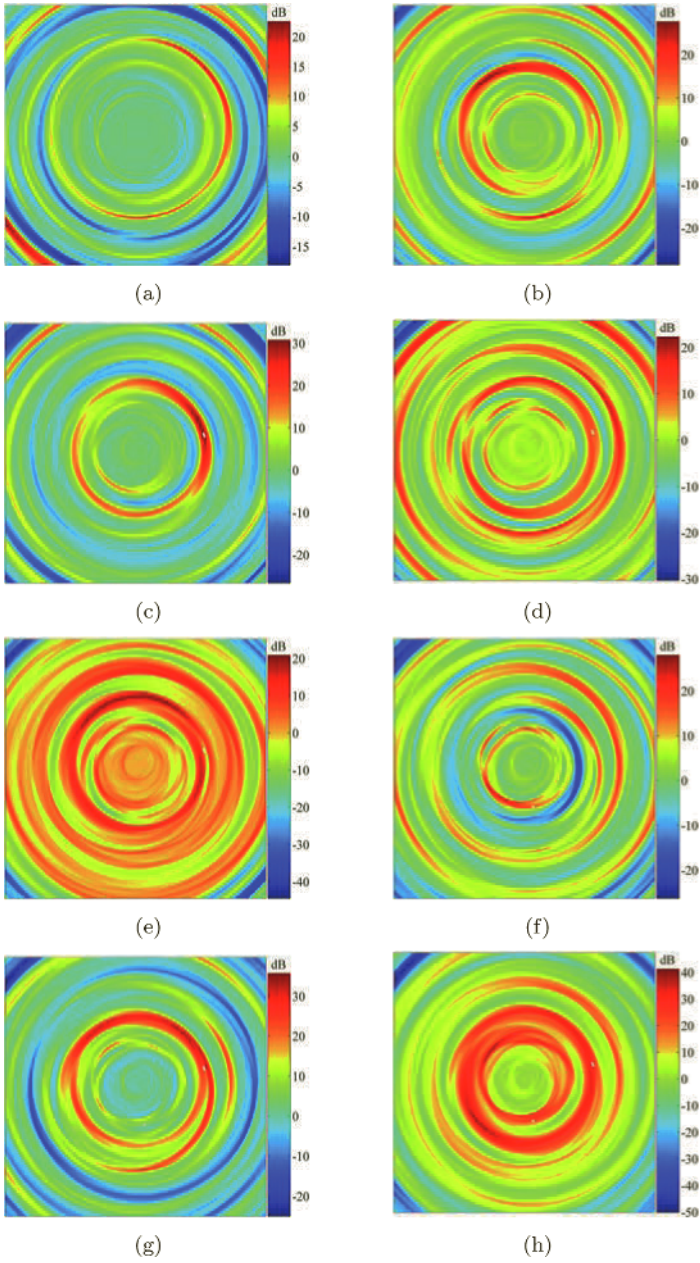
Figure 26. Experiment: damage influence maps.

location of the delamination is much more difficult. It derives from the fact that amplitudes of waves reflected from delamination are significantly lower than amplitudes of waves reflected from cracks.
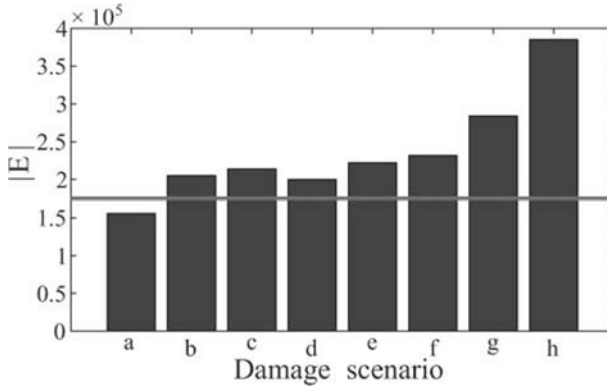
Figure 27. Damage size indicator.

6.6   Conclusions

Analyses of signals measured with the use of specialist testing equipment were conducted. Estimation of wave group velocities for various frequencies and numbers of cycles was made. Dispersion curves, and profiles of dependence of wave group velocities on the angle of propagation, were calculated. Experimental results were compared with theoretical results. High conformity between theory and experiment both in dispersion curves and profiles of velocity depending on wave propagation angle were observed.

A serious problem with the studied specimen of a composite structure is the high damping, which increases in proportion to the frequency of the excitation signal.

The developed damage detection algorithm enables detection of extremely small cracks. In some cases, it is also possible to locate the crack.

Bibliography

URL http://www.performance-composites.com.

D.N. Alleyne and P. Cawley. Optimization of Lamb wave inspection techniques. *NDT&E International*, 25:11–22, 1992.

K. Amaratunga and J.R. Williams. Time integration using wavelets. In *Proceedings of SPIE, Wavelet Application for Dual Use*, pages 894–902, 1995.

A. Bachschmid, G. Diana, and B. Pizzigoni. The influence of unbalance on cracked rotors. In *Vibrations of Rotating Machinery*, pages 193–198. Institution of Mechanical Engineers, 1984.

L.J. Bond. Numerical techniques and their use to study wave propagation and scattering: a review. In S.K. Datta, J.D. Achenbach, and Y.S. Rajapakse, editors, *Elastic Waves and Ultrasonic Non-destructive Evaluation*. North-Holland, 1990. The Proceedings of the IUTAM Symposium.

J.P. Boyd. *Chebyshev and Fourier spectral methods*. Springer, 1989.

C. Canuto, M.Y. Hussaini, A. Quarteroni, and T.A. Zang. *Spectral methods in fluid dynamics*. Springer, 3 edition, 1991.

P. Cawley and R.D. Adams. The location of defects in structures from measurements of natural frequencies. *Journal of Strain Analysis*, 14: 49–57, 1979.

A. Chakraborty and S. Gopalakrishnan. A spectrally formulated finite element for wave propagation analysis in layered composite media. *International Journal of Solids and Structures*, 41:5155–5183, 2004.

A. Chakraborty and S. Gopalakrishnan. A spectrally formulated plate element for wave propagation analysis in anisotropic material. *Computer Methods in Applied Mechanics and Engineering*, 194:4425–4446, 2005.

A. Chakraborty and S. Gopalakrishnan. A spectral finite element model for wave propagation analysis in laminated composite plate. *Journal of Vibration and Acoustics*, 128:477–488, 2006a.

A. Chakraborty and S. Gopalakrishnan. An approximate spectral element for the analysis of wave propagation in inhomogeneous layered media. *AIAA Journal*, 44:1676–1685, 2006b.

L.W. Chen and C.L. Chen. Vibration and stability of cracked thick rotating blades. *Computers and Structures*, 28:67–74, 1988.

Y.K. Cheung. *Finite Strip Method in Structural Mechanics*. Pergamon Press, Oxford, 1976.

A.J Chipperfield, P.J. Fleming, H. Pohlheim, and C.M. Fonseca. Genetic algorithm toolbox user's guide. ACSE Research Report 512, University of Sheffield, 1994.

Y. Cho and J.L. Rose. A boundary element solution for a mode conversion study on the edge reflection of lamb waves. *Journal of the Acoustical Society of America*, 99(4):2079–2109, 1996.

W. Dauksher and A.F. Emery. Accuracy in modeling the acoustic wave equation with Chebyshev spectral finite elements. *Finite Elements in Analysis and Design*, 26:115–128, 1997.

P.P. Delsanto, T. Whitecomb, H.H. Chaskelis, and R.B. Mignogna. Connection machine simulation of ultrasonic wave propagation in materials I: the one-dimensional case. *Wave Motion*, 16:65–80, 1992.

P.P. Delsanto, T. Whitecomb, H.H. Chaskelis, R.B. Mignogna, and R.B. Kline. Connection machine simulation of ultrasonic wave propagation in materials II: the two-dimensional case. *Wave Motion*, 20:295–314, 1994.

P.P. Delsanto, R.S Schechter, and R.B. Mignogna. Connection machine simulation of ultrasonic wave propagation in materials III: The three-dimensional case. *Wave Motion*, 26:329–339, 1997.

J.F. Doyle. *Wave Propagation in Structures*. Springer-Verlag, 2 edition, 1997.

D. E. Goldberg. *Genetic Algorithms in Search, Optimization and Machine Learning*. Kluwer Academic Publishers, Boston, 1989.

G. Gounaris and A.D. Dimarogonas. A finite element a cracked prismatic beam for structural analysis. *Computers and Structures*, 28:309–313, 1988.

B.S. Haisty and W.T. Springer. A general beam element for use in damage assessment of complex structures. *Journal of Vibration, Acoustics, Stress, and Reliability in Design*, 110:389–394, 1988.

Y. Kim, S. Ha, and F.-K. Chang. Time–domain spectral element method for built–in piezoelectric–actuator–induced Lamb wave propagation analysis. *AIAA Journal*, 46(3):591–600, 2008.

D. Komatitsch and J.P. Vilotte. The spectral element method: An efficient tool to simulate the seismic response of 2D and 3D geological structures. *Bulletin of the Seismological Society of America*, 88:368–392, 1998.

D. Komatitsch, Ch. Barnes, and J. Tromp. Simulation of anisotropic wave propagation based upon a spectral element method. *Geophisics*, 65(4): 1251–1260, 2000.

M. Koshiba, S. Karakida, and M. Suzuki. Finite element analysis of Lamb waves scattering in an elastic plate waveguide. *IEEE Transactions on Sonic and Ultrasonic*, 31:18–25, 1984.

M. Krawczuk. Modelling and identification of cracks in truss constructions. *Finite Element Analysis and Design*, 12:41–50, 1992.

M. Krawczuk. A rectangular plate finite element with an open crack. *Computers and Structures*, 46:487–493, 1993.

M. Krawczuk. Rectangular shell finite element with an open crack. *Finite Elements in Analysis and Design*, 15:233–253, 1994.

M. Krawczuk and W. Ostachowicz. Identification of delamination in composite beams by genetic algorithm. *Science and Engineering of Composite Materials*, 10(2):147–155, 2002.

M. Krawczuk and W. Ostachowicz. Hexahedral finite element with an open crack. *Finite Elements in Analysis and Design*, 13:225–235, 1993a.

M. Krawczuk and W. Ostachowicz. A finite plate element for dynamic analysis of a cracked plate. *Computer Methods in Applied Mechanics and Engineering*, 115:67–78, 1994.

M. Krawczuk and W. Ostachowicz. Journal of vibration and acoustics. *Natural vibrations of a clampedclamped arch with an open transverse crack*, 119:145–151, 1997.

M. Krawczuk and W.M. Ostachowicz. Transverse natural vibrations of a cracked beam loaded with a constant axial force. *Journal of Vibration and Acoustics*, 115:524–528, 1993b.

M. Krawczuk, W. Ostachowicz, and A. Zak. Modal analysis of cracked, unidirectional composite beam. *Composites Part B: Engineering*, 28B: 641–650, 1997.

M. Krawczuk, A. Zak, and W. Ostachowicz. Elastic beam finite element with a transverse elastoplastic crack. *Finite Elements in Analysis and Design*, 341(1):61–73, 2000.

M. Krawczuk, A. Zak, and W. Ostachowicz. Finite element model of plate with elastoplastic through crack. *Computers and Structures*, 79:515–532, 2001.

M. Krawczuk, M. Palacz, and W. Ostachowicz. The dynamic analysis of cracked Timoshenko beam by the spectral element method. *Journal of Sound and Vibration*, 264:11391153, 2003.

M. Krawczuk, M. Palacz, and W. Ostachowicz. Flexural-shear wave propagation in cracked composite beam. *Science and Engineering of Composite Materials*, 11:55–67, 2004.

P. Kudela. *Damage detection in selected composite elements of structures by the elastic wave propagation method*. PhD thesis, Polish Academy of Sciences, Institute of Fluid-Flow Machinery, 2008. in polish.

P. Kudela and W. Ostachowicz. Damage detection in composite rods by the elastic wave propagation method. In *Computer Methods in Mechanics*, 2007.

P. Kudela, W. Ostachowicz, and A. Żak. Influence of temperature fields on wave propagation in composite plates. In *Key Engineering Materials*, volume 347, pages 537–542, Switzerland, 2007a. Trans Tech Publications.

P. Kudela, A. Żak, M. Krawczuk, and W. Ostachowicz. Modelling of wave propagation in composite plates using the time domain spectral element method. *Journal of Sound and Vibration*, 302:728745, 2007b.

P. Kudela, W. Ostachowicz, and A. Żak. Damage detection in composite plates with embedded PZT transducers. *Mechanical Systems and Signal Processing*, 22:1327–1335, 2008.

B.C. Lee, M. Palacz, M. Krawczuk, W. Ostachowicz, and W.J. Staszewski. Wave propagation in a sensor/actuator diffusion bond model. *Journal of Sound and Vibration*, 276:671–687, 2004.

G.R. Liu and Z.C. Xi. *Elastic waves in anisotropic laminates*. CRC Press, 2002.

G.R. Liu, J. Tani, K. Watanabe, and T. Ohyoshi. Harmonic wave propagation in anisotropic laminated strips. *Journal of Sound and Vibration*, 139:313–330, 1990.

T. Liu, K. Liu, and J. Zhang. Unstructured grid method for stress wave propagation in elastic media. *Computer Methods in Applied Mechanics and Engineering*, 193:2427–2452, 2004.

T. Liu, K. Liu, and J. Zhang. Triangular grid method for stress-wave propagation in 2–D orthotropic materials. *Archive of Applied Mechanics*, 74: 477–488, 2005.

D.R. Mahapatra and S. Gopalakrishnan. A spectral finite element model for analysis of axialflexuralshear coupled wave propagation in laminated composite beams. *Computers and Structures*, 59:67–88, 2003.

M. Mitra and S. Gopalakrishnan. Wavelet based spectral finite element for analysis of coupled wave propagation in higher order composite beams. *Composite Structures*, 73:263–277, 2006.

W. Ostachowicz and M. Krawczuk. On modelling of structural stiffness loss due to damage. In *Key Engineering Materials*, volume 204-205, page 185200, 2001.

W. Ostachowicz and M. Krawczuk. Coupled torsional and bending vibrations of a rotor with an open crack. *Archive of applied mechanics*, 62: 191–201, 1992.

W. Ostachowicz, M. Krawczuk, and M.P. Cartmell. The location of a concentrated mass on rectangular plates from measurements of natural vibrations. *Computers and Structures*, 80:1419–1428, 2002.

W. Ostachowicz, M. Krawczuk, and M. Palacz. Detection of delamination in multilayer composite beams. In *Key Engineering Materials*, pages 245–246, 2003.

M. Palacz and M. Krawczuk. Analysis of longitudinal wave propagation in a cracked rod by the spectral element method. *Computers and Structures*, 80:1809–1816, 2002.

A.T. Patera. A spectral element method for fluid dynamics: Laminar flow in a channel expansion. *Journal of Computational Physics*, 54:468–488, 1984.

C. Pozrikidis. *Introduction to Finite and Spectral Element Methods using MATLAB(R)*. Chapman & Hall/CRC, 2005.

J.S. Przemieniecki. *Theory of matrix structural analysis*. McGraw Hill, New York, 1968.

G.L. Qian, S.N. Gu, and J.S. Jiang. A finite element model of cracked plates and application to vibration problems. *Computers and Structures*, 39: 483–487, 1991.

X.P. Qing, H-L. Chan, S.J. Beard, T.K. Ooi, and S.A. Marotta. Effect of adhesive on the performance of piezoelectric elements used to monitor structural health. *International Journal of Adhesion & Adhesives*, 26: 622–628, 2006.

E. Ruffino and P.P Delsanto. Problems of accuracy and reliability in 2–D LISA simulations. *Computers and Mathematics with Applications*, 38: 89–97, 1999.

R.S. Schechter, H.H. Chaskelis, R.B. Mignogna, and P.P. Delsanto. Real-time parallel computation and visualization of ultrasonic pulses in solids using the connection machine. *Science*, 265:1188–1192, 1994.

G. Seriani. A parallel spectral element method for acoustic wave modeling. *Journal of Computational Acoustics*, 5(1):53–69, 1997.

G. Seriani. 3–D spectral element-by-element wave modelling on Cray T3E. *Physics and Chemistry of the Earth*, 24(3):241–249, 1999.

R. Spall. Spectral collocation methods for one dimensional phase change problems. *International Journal of Heat Mass Transfer*, 15:2743–2748, 1995.

R. Sridhar, A. Chakraborty, and S. Gopalakrishnan. Wave propagation in anisotropic and inhomogeneous uncracked and cracked structures using pseudospectral finite element method. *International Journal of Solids and Structures*, 43:4997–5031, 2006.

J.C. Strickwerda. *Finite Difference Schemes and Partial Differential Equations*. Wadsworth-Brooks, 1989.

H. Tada, P.C. Paris, and G.R. Irwin. *The stress analysis of cracks handbook*. Del Research Corporation, 1973.

G.S. Verdict, P.H. Gienand, and C.P. Burger. Finite element study of Lamb wave interactions with holes and through thickness defects in thin metal plates. *Review of Progress in Quantitative Non-destructive Evaluation*, 11:97–104, 1992.

J.R. Vinson and R.L. Sierakowski. *Behaviour of Stuctures Composed of Composite Materials*. Martinus Nijhoff, Dorchester, 3rd edition, 1989.

H. Yamawaki and T. Saito. Numerical calculation of surface waves using new nodal equation. *NDT&E International*, 8-9:379–389, 1992.

H. Yim and Y. Sohn. Numerical simulation and visualization of elastic waves using mass-spring lattice model. *IEEE Transaction on Ultrasonics, Ferroelectrics, and Frequency Control*, 47(3):549–558, 2000.

M.M.F. Yuen. A numerical study of the eigenparameters of damaged cantilever beam. *Journal of Sound and Vibration*, 103:301–310, 1985.

A. Żak, M. Krawczuk, and W. Ostachowicz. Numerical and experimental investigation of free vibration of multilayer delaminated composite beams and plates. *Computational Mechanics*, 26:309–315, 2000.

A. Zak, M. Krawczuk, and W. Ostachowicz. Vibration of a laminated composite plate with closing delamination. *Journal of Intelligent Material Systems and Structures*, 12(8):545–551, 2001.

A. Żak, M. Krawczuk, and W. Ostachowicz. Propagation of in-plane waves in an isotropic panel with a crack. *Finite Elements in Analysis and Design*, 42:929–941, 2006.

A. Żak, M. Krawczuk, W. Ostachowicz, P. Kudela, and M. Palacz. Elastic wave propagation in cracked isotropic plates. In *Proceedings of the Third European Workshop Structural Health Monitoring 2006*, pages 316–323, 2006.

A.J. Zak, M.P. Cartmell, and W.M. Ostachowicz. A sensitivity analysis of the dynamic performance of a composite plate with shape memory alloy wires. *Composite Structures*, 60:145–157, 2003.